Nearly Inviscid Faraday Waves

Edgar Knobloch
José M. Vega

ABSTRACT Many powerful techniques from Hamiltonian mechanics are available for the study of ideal hydrodynamics. This article explores some of the consequences of including small viscosity in a study of surface gravity-capillary waves excited by the vertical vibration of a container. It is shown that in this system, as in others, the addition of small viscosity provides a singular perturbation of the ideal fluid problem, and that as a result its effects are nontrivial. The relevance of existing studies of ideal fluid problems is discussed from this point of view.

Contents

1 Introduction

Jerry Marsden has been a driving force in studies of ideal hydrodynamics using methods from Hamiltonian mechanics. Perhaps his most important contribution has been the discovery of a systematic procedure for the construction of noncanonical Hamiltonian structures for such flows. The required noncanonical Poisson brackets are typically singular, implying the

presence of additional conserved quantities known as Casimirs. Using these techniques he and his colleagues were able to extend Arnol'd-type stability theorems to a number of flows of importance in geophysics and engineering (Marsden and Morrison [1984]; Holm, Marsden, Ratiu, and Weinstein [1985]; Abarbanel, Holm, Marsden, and Ratiu [1986]; Holm, Marsden, and Ratiu [1986]; Lewis, Marsden, Montgomery, and Ratiu [1986]). These are major contributions to the field of ideal hydrodynamics and are nowadays taught in graduate level courses on the subject.

Although these techniques are powerful, and enable one to obtain results that would be hard to obtain by other means, there remains an important question as to their relevance to flows in the real world. Unless one studies flows in a superfluid, for example ^{4}He below the λ-point (i.e., at temperatures below the transition to superfluidity) such flows are inevitably affected by dissipative processes, be they viscous or thermal. These may have an importance beyond being responsible for the decay of the flow on the slow diffusive time scale (Batchelor [1967]; Chorin and Marsden [1979]). In general the presence of small viscosity is responsible for the formation of thin boundary layers where the flow departs drastically from that in the bulk. In such boundary layers vorticity is generated by viscous effects and this vorticity may then diffuse or be convected into the bulk. In such cases the flow in the bulk may be substantially modified. Boundary layers may be classified as passive or dynamic, depending on their effect on the bulk flow. Passive boundary layers do not affect the flow in the bulk, which will then resemble the potential solution over long times; such boundary layers serve merely to adjust the flow to the physically relevant boundary conditions. In the absence of boundary layer separation such boundary layers are found, for example, in steady flow around obstacles. Oscillatory boundary layers may likewise be passive if the oscillation amplitude is small and only the leading order oscillatory flow is considered. However, as discussed further below, this is no longer so at second order in amplitude. In this and other cases the boundary layers can become dynamic, and force the flow in the bulk even though this flow remains largely inviscid. In such cases the inviscid flow in the bulk differs substantially from the flow that would be obtained by ignoring the boundary layers altogether, and this effect persists in the limit in which the viscosity vanishes, i.e., in these cases the limit of vanishing viscosity may have at most a tenuous connection with the behavior of the strictly inviscid system (Batchelor [1967]). The present article is devoted to the explication of this phenomenon in the context of a particularly interesting physical system, gravity-capillary waves in a vertically vibrating container (the Faraday system).

The difference between the properties of the Euler equation for an ideal incompressible fluid and the Navier–Stokes equation in the limit of large Reynolds number provides the most famous example of the dangers of ignoring viscosity entirely, in the sense that the 'thermodynamic equilibrium' spectrum that results bears no relation to the energy spectrum in

the so-called inertial range. But there are simple examples of problems not involving turbulence where viscosity, however small, also plays a profound role. Perhaps the simplest is provided by the computation of the Lagrangian drift of a fluid element when a surface gravity-capillary wave passes overhead. This drift is important because its sum over all the fluid elements may be identified with the *linear momentum* associated with the wave (Knobloch and Pierce [1998], and references therein). In the following we employ Cartesian coordinates, with the x-axis along the unperturbed free surface of the fluid and y vertically upwards. An irrotational incompressible flow then satisfies the equation

$$\nabla^2 \phi = 0,$$

where $\mathbf{u} \equiv (\phi_x, \phi_y)$ is the Eulerian velocity, subject to the boundary conditions

$$\phi_y = 0 \quad \text{at } y = -h;$$
$$f_t + \phi_x f_x = \phi_y, \quad \phi_t + |\mathbf{u}|^2/2 + p/\rho + gf = 0 \quad \text{at } y = f.$$

Here f is the free surface deflection, $p = p_0 - T f_{xx}(1 + f_x^2)^{-3/2}$, the excess pressure being a consequence of the presence of the surface tension T, and g and ρ are, respectively, the acceleration due to gravity and the fluid density. A formulation of this type assumes that the fluid remains irrotational if it is irrotational initially. This is so only if the fluid is *strictly* inviscid.

Since a particle starting at $\mathbf{x} = \mathbf{a}$ at $t = 0$ is at

$$\mathbf{x} = \mathbf{a} + \int_0^t \mathbf{v}(\mathbf{a}, t')\, dt'$$

at time t, the Lagrangian velocity of the fluid element at time t is given, to second order, by

$$\mathbf{v}(\mathbf{a}, t) = \mathbf{u}(\mathbf{a}, t) + \left(\int_0^t \mathbf{u}(\mathbf{a}, t') dt' \right) \cdot \nabla_{\mathbf{a}} \mathbf{u}(\mathbf{a}, t).$$

For a progressive sinusoidal wave of (small) amplitude A, $f = A\cos(kx - \omega t) + O(A^2)$ and $\phi = [f_t \cosh k(y+h)]/k \sinh kh + O(A^2)$. If A is constant in space it is possible to show that the time-averaged Eulerian velocity $\langle \mathbf{u} \rangle$ vanishes to second order but the time-averaged Lagrangian drift $\langle \mathbf{v} \rangle$ does not:

$$\langle \mathbf{v} \rangle = \left(\frac{\omega k A^2 \cosh\ 2k(y+h)}{2 \sinh^2 kh}, 0 \right). \tag{1.2}$$

This drift is known as the ***Stokes drift***. However, in the presence of small viscosity, this result is misleading. The argument that follows goes back to the work of Schlichting [1932]. Observe that for sufficiently small viscosity (namely $\beta h \gg 1$, $\beta/k \gg 1$, where $\beta = (\omega/2\nu)^{1/2}$) the inviscid solution

applies everywhere except in the two thin oscillatory viscous boundary layers of $O(\beta^{-1})$ thickness along the top and bottom, whose contribution can be superposed on top of the irrotational flow just computed. Therefore, if in the bottom boundary layer we write $\mathbf{u} = \nabla\phi + \mathbf{u}'$, then at leading order $\mathbf{u}' = (u', v')$ satisfies the linearized *vorticity* equation

$$\frac{\partial \Omega}{\partial t} = \nu\left(\frac{\partial^2 \Omega}{\partial x^2} + \frac{\partial^2 \Omega}{\partial y^2}\right), \qquad \Omega = \nabla \times \mathbf{u}',$$

subject to the boundary conditions

$$u' = -\phi_x, \quad v' = 0 \text{ at } y = -h; \quad u' = 0 \text{ for } \beta(y+h) \gg 1.$$

This problem has the solution

$$u' = -\omega A \operatorname{cosech} kh \, \mathrm{e}^{-\beta(y+h)} \cos\bigl(kx - \omega t + \beta(y+h)\bigr),$$
$$v' = -\int_{-h}^{y} [\partial u'(x,z,t)/\partial x]\, dz.$$

With these expressions it is possible to compute a time-averaged Reynolds stress in the oscillatory boundary layer,

$$\langle u'v' \rangle = \frac{\omega^2 k A^2}{4\beta \sinh^2 kh}\left[2(\beta\tilde{y}\sin\beta\tilde{y} + \cos\beta\tilde{y})\mathrm{e}^{-\beta\tilde{y}} - \mathrm{e}^{-2\beta\tilde{y}} - 1\right],$$

correct to second order in the wave amplitude A. Here $\tilde{y} \equiv y + h$. This Reynolds stress drives a mean flow $(U'(y), 0)$ according the mean momentum equation $\nu\partial^2 U'/\partial y^2 = \partial\langle u'v'\rangle/\partial y$, i.e.,

$$\nu \frac{\partial U'}{\partial y} = \langle u'v' \rangle \quad \langle u'v' \rangle_\infty, \tag{1.5}$$

where $\langle u'v' \rangle_\infty$ represents the Reynolds stress just outside of the boundary layer. Letting $\beta(y+h) \to \infty$ one finds that

$$\langle u'v' \rangle_\infty = -\omega^2 k A^2/(4\beta \sinh^2 kh).$$

In view of the requirement $U'(-h) = 0$ equation (1.5) now implies that

$$U'(y) \to U'_\infty = \frac{3\omega k A^2}{4\sinh^2 kh} \qquad \text{for } \beta(y+h) \gg 1.$$

Thus the time-averaged Eulerian velocity at the edge of the boundary layer is (a) *finite* at second order, and (b) *independent* of ν (for sufficiently small ν), provided only that $\nu > 0$! Since this Eulerian mean flow also carries the fluid elements with it its effect must be added to the Stokes drift (1.2) computed on the basis of inviscid theory. Thus the net Lagrangian drift for $\beta h \gg 1$, $\beta/k \gg 1$ is in fact

$$\langle \mathbf{v} \rangle_\infty = \left(\frac{5\omega k A^2}{4\sinh^2 kh}, 0\right),$$

a value that is 5/2 times the inviscid value (Longuet-Higgins [1953]; Batchelor [1967]; Phillips [1977]; Craik [1982]). As recognized already by Longuet-Higgins [1953], a somewhat similar effect is present at the free surface as well. It is clear therefore that the oscillatory viscous boundary layers *must* be retained even in the limit of arbitrarily small viscosity, and that these are effective at driving large scale mean flows even when the viscosity ν is arbitrarily small.

In the following we discuss in some detail the corresponding phenomena in the Faraday system, where oscillatory viscous boundary layers are inevitably present, and explore the interaction between the Faraday instability and the mean flow driven in these boundary layers. In systems of small to moderate aspect ratio such mean flows are entirely of viscous origin (Nicolás and Vega [1996]; Higuera, Nicolás, and Vega [2000]), but in the larger aspect ratio systems of interest below the situation is rather more subtle because of the presence of an additional *inviscid mean flow*. For inviscid free waves this mean flow is associated with spatial modulation of a single mode, as described by the celebrated Davey-Stewartson equations (Davey and Stewartson [1974]; Pierce and Knobloch [1994]). If viscosity is retained and the system forced, as in a shear flow, a similar set of equations but with complex coefficients can be derived (Davey, Hocking, and Stewartson [1974]). In general the mean flow present will contain both viscous and inviscid contributions, even in nearly inviscid flows. It is because of these effects that one cannot mimic the effects of viscosity on an oscillating fluid system by simply adding dissipation *post facto* to an otherwise inviscid theory.

2 The Faraday System

Surface gravity-capillary waves excited parametrically by the vertical oscillation of a container provide a convenient and well-studied system (Miles and Henderson [1990]; Fauve [1995]; Kudrolli and Gollub [1997]), where the issues raised in the preceding section come to the fore. We nondimensionalize distances with the unperturbed depth h and time with the gravity-capillary time $[g/h+T/(\rho h^3)]^{-1/2}$. In two dimensions the resulting viscous problem is then described by the dimensionless equations (Vega, Knobloch, and Martel [2001]),

$$\psi_{xx}+\psi_{yy}=\Omega, \quad \Omega_t-\psi_y\Omega_x+\psi_x\Omega_y=C_g(\Omega_{xx}+\Omega_{yy}), \tag{2.1}$$

$$f_t-\psi_x-\psi_y f_x=(\psi_{yy}-\psi_{xx})(1-f_x^2)-4f_x\psi_{xy}=0 \quad \text{at } y=f, \tag{2.2}$$

$$\begin{aligned}(1-S)f_x-S(f_x/\sqrt{1+f_x^2})_{xx}-\psi_{yt}+\psi_{xt}f_x-(\psi_x+\psi_y f_x)\Omega\\ +(\psi_x^2+\psi_y^2)_x/2+(\psi_x^2+\psi_y^2)_y f_x/2-4\mu\omega^2\cos(2\omega t)f_x\\ =-C_g[3\psi_{xxy}+\psi_{yyy}-(\psi_{xxx}+\psi_{xyy})f_x]\end{aligned}$$

$$+ 2C_g \left[\frac{2\psi_{xy} f_x^2 - (\psi_{xx} - \psi_{yy}) f_x}{1 + f_x^2} \right]_x$$
$$+ 2C_g \frac{(\psi_{xxy} - \psi_{yyy}) f_x^2 - \psi_{xyy}(1 - f_x^2) f_x}{1 + f_x^2} \quad \text{at } y = f\,, \tag{2.3}$$

$$\int_0^L \Omega_y \, dx = \psi = \psi_y = 0 \quad \text{at } y = -1, \qquad \int_0^L f \, dx = 0\,, \tag{2.4}$$

where ψ is the streamfunction, defined such that $\mathbf{u} \equiv (-\psi_y, \psi_x)$ is the velocity, $\Omega \equiv \nabla \times \mathbf{u}$ is the vorticity, and f is again the free surface deflection. The latter is required to satisfy volume conservation as in (2.4d). In an annular container of dimensionless length L periodic boundary conditions are applied to all quantities; in this case the boundary condition (2.4a) guarantees that the pressure is also periodic in x. The resulting problem depends on

L	the aspect ratio,
μ	the nondimensional vibration amplitude,
2ω	the nondimensional vibration frequency,
$C_g = \nu/[gh^3 + (Th/\rho)]^{1/2}$	the capillary-gravity number,
$S = T/(T + \rho g h^2)$	the gravity-capillary balance parameter.

Here ν is the kinematic viscosity. Thus C_g and S are related to the usual capillary number $C = \nu[\rho/Th]^{1/2}$ and the Bond number $B = \rho g h^2/T$ by

$$C_g = C/(1 + B)^{1/2} \quad \text{and} \quad S = 1/(1 + B).$$

Note that $0 \leq S \leq 1$ and that the extreme values $S = 0, 1$ correspond to the purely gravitational ($T = 0$) and the purely capillary ($g = 0$) limits, respectively.

The formulation employed above uses the streamfunction ψ and not the velocity potential ϕ, since formulations of the Faraday problem in terms of the latter miss both the mechanism for the generation of (Eulerian) mean flows already discussed in §1, and the possibility that vorticity will diffuse from the viscous boundary layers along walls and the free surface into the nominally inviscid interior. These boundary layers form because in the presence of viscosity the tangential velocity must vanish along any wall while the tangential stress along the free surface is also required to vanish. Neither of these two effects is restored by the *a posteriori* addition of damping to a fundamentally inviscid formulation, i.e., a formulation based on the velocity potential. In fact, for times that are not too long the vorticity contamination of the bulk does remain negligible, so that the flow in the bulk is correctly described by an inviscid formulation but with boundary conditions determined by a boundary layer analysis as in §1.

The basic assumption made below is that viscosity is small, namely

$$C_g \ll 1. \tag{2.5}$$

However, as already mentioned, this does not mean that viscous effects can be safely ignored. Indeed, the subtleties arise already at the level of the linear problem. The normal modes of the unforced problem, linearized around $\psi = f = 0$, take the form

$$(\psi, f) = (\Psi, F)e^{\lambda t + \mathrm{i}kx}.$$

In the limit (2.5) there are two types of such modes (Kakutani and Matsuuchi [1975]; Martel and Knobloch [1997]):

A. The *nearly inviscid modes* (or surface modes) obey the dispersion relation

$$\lambda = \mathrm{i}\omega - (1-\mathrm{i})\alpha_1 C_g^{1/2} - \alpha_2 C_g + O(C_g^{3/2}), \tag{2.7}$$

where

$$\begin{aligned} \omega &= [k\sigma(1 - S - Sk^2)]^{1/2}, \\ \alpha_1 &= \frac{k(\omega/2)^{1/2}}{\sinh(2k)}, \\ \alpha_2 &= \frac{k^2}{4\sigma^2}(1 + 8\sigma^2 - \sigma^4), \end{aligned} \tag{2.8}$$

and $\sigma \equiv \tanh k$. Eq. (2.7) provides a good approximation for both the frequency $\pm\mathrm{Im}(\lambda)$ and the damping rate,

$$\delta \equiv -\mathrm{Re}(\lambda) = \alpha_1 C_g^{1/2} + \alpha_2 C_g, \tag{2.9}$$

for small but fixed values of C_g, see Fig. 2.1. However, as noted in Martel and Knobloch [1997], if the (corrected) third term in (2.7) is omitted the resulting approximation breaks down as soon as $k \gtrsim k_m \sim |\ln C_g|$. Since these moderately large values of k are also of interest this term is retained in what follows.

The eigenfunction associated with the dispersion relation (2.7) is given (up to a constant factor) by

$$(\Psi, F) = (\Psi_0, 1) + O(C_g^{1/2}), \quad \Psi_0 = \frac{\omega \sinh[k(y+1)]}{k \sinh k}.$$

These modes therefore exhibit a significant free-surface deflection; moreover, they are irrotational in the bulk, outside two thin boundary layers of thickness $O((C_g/\omega)^{1/2})$ attached to the bottom plate and the free surface. Since the decay rate of these modes is $O(C_g^{1/2})$ for small C_g these modes are near-marginal in nearly inviscid fluids. Note that the horizontal wavenumber k is only restricted by the periodicity condition and thus can take any value of the form $2\pi N/L$, where N is an integer; in the limit $L \to \infty$ the allowed wavenumbers become dense on the real line. In the following we assume that the basic disturbance consists of a pair of counterpropagating wavetrains with wavenumber $\pm k$ and frequency ω determined from the above dispersion relation, and that the mean flow arises from nonlinear

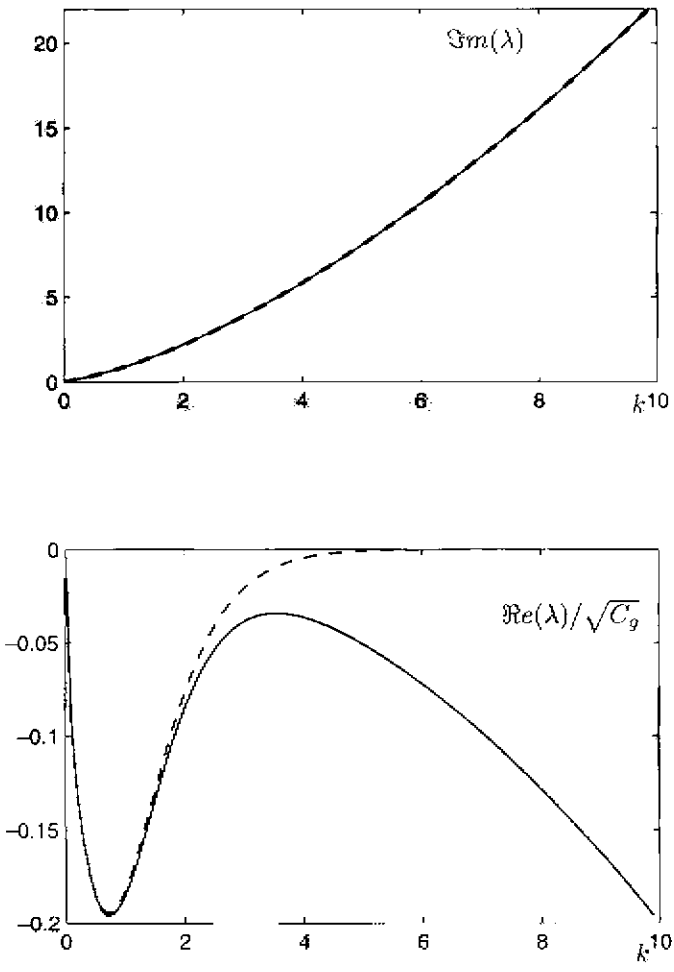

FIGURE 2.1. The nearly inviscid dispersion relation, $\Im m\,\lambda$ and $\Re e\,\lambda$ vs. k, for $C_g = 10^{-6}$, $S = 0.5$, from Eq. (2.7) using the $O(C_g^{1/2})$ results (dashed line) and the $O(C_g)$ results (solid line). These parameters correspond to the experiments of Henderson and Miles [1994].

interactions involving these two modes. Here ω represents half the forcing frequency. Thus the relevant nearly inviscid modes are either of long wavelength ($k \to 0$) or are concentrated around the two counterpropagating modes. The long wave modes constitute the *nearly inviscid* mean flow; in the strictly inviscid case, this flow is the mean flow considered in inviscid theories (Davey and Stewartson [1974]; Pierce and Knobloch [1994]). However, because of its long wavelength this mean flow does not appear if the aspect ratio is of order unity (Nicolás and Vega [1996]; Higuera, Nicolás,

and Vega [2000]).

B. The *viscous modes* (or hydrodynamical modes) obey the dispersion relation

$$\lambda = -C_g[k^2 + q_n(k)^2] + O(C_g^2),$$

where for each $k > 0$, $q_n > 0$ is the n-th root of $q \tanh k = k \tan q$, and hence decay on an $O(C_g)$ timescale, i.e., more slowly than the surface modes when C_g is sufficiently small. Consequently these modes are also near-marginal. Since the associated eigenfunction is

$$\Psi = \sin q_n \sinh(ky) - \sinh k \sin(q_n y) - O(C_g), \quad F = O(C_g),$$

these modes do not result in any significant free-surface deformation at leading order. On the other hand they are rotational throughout the domain and, when forced at the edge of the oscillatory boundary layers along the bottom (Schlichting [1932]) and the free surface (Longuet–Higgins [1953]) by the mechanism described in §1, they constitute the viscous mean flow. In view of its slow decay this flow must be included in any realistic nearly inviscid description.

With this in mind it is now possible to perform a multiscale analysis of the viscous fluid equations using C_g, L^{-1} and μ as unrelated small parameters. We focus on two well-separated scales in both space ($x \sim 1$ and $x \gg 1$) and time ($t \sim 1$ and $t \gg 1$), and derive equations for small, slowly-varying amplitudes A and B of left- and right-propagating waves. Since viscosity is small, we must distinguish three regions in the physical domain, namely, the two oscillatory boundary layers (of thickness $O(C_g^{1/2})$) and the remaining part (or *bulk*) of the domain (see Fig. 2.2). The boundary layers must be considered in order to obtain the correct boundary conditions for the solution in the bulk. The details of the derivation are quite involved and can be found in a recent paper (Vega, Knobloch, and Martel [2001]), where explicit conditions for the validity of the resulting equations as a description of the two-dimensional nearly inviscid Faraday system are also derived. The resulting equations take the form

$$A_t - v_g A_x = \mathrm{i}\alpha A_{xx} - (\delta + \mathrm{i}d)A + \mathrm{i}(\alpha_3|A|^2 - \alpha_4|B|^2)A + \mathrm{i}\alpha_5\mu\bar{B} + \mathrm{i}\alpha_6 \int_{-1}^{0} g(y)\langle \psi_y^m \rangle^x \, dy \, A + \mathrm{i}\alpha_7 \langle f^m \rangle^x A, \tag{2.11}$$

$$B_t + v_g B_x = \mathrm{i}\alpha B_{xx} - (\delta - \mathrm{i}d)B + \mathrm{i}(\alpha_3|B|^2 - \alpha_4|A|^2)B + \mathrm{i}\alpha_5\mu\bar{A} - \mathrm{i}\alpha_6 \int_{-1}^{0} g(y)\langle \psi_y^m \rangle^x \, dy \, B - \mathrm{i}\alpha_7 \langle f^m \rangle^x B, \tag{2.12}$$

$$A(x + L, t) \equiv A(x, t), \quad B(x + L, t) \equiv B(x, t), \tag{2.13}$$

where μ denotes the (small) amplitude of the periodic forcing. The first seven terms in these equations, accounting for inertia, propagation at the group velocity v_g, dispersion, damping, detuning, cubic nonlinearity and

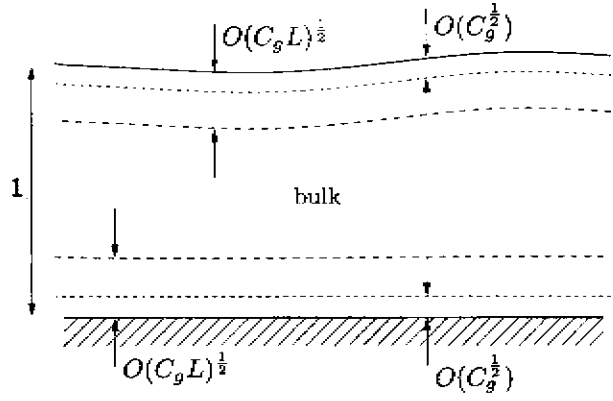

FIGURE 2.2. Sketch of the primary and secondary boundary layers, indicating their widths in comparison to the layer depth.

parametric forcing, are familiar from existing weakly nonlinear, nearly inviscid theories (Ezerskii, Rabinovich, Reutov, and Starobinets [1986]). These theories lead to expression (2.9) for the damping δ and the expressions

$$v_g = \omega'(k), \qquad \alpha = \omega''(k)/2, \tag{2.14}$$

$$\alpha_3 = \frac{\omega k^2[(1-S)(9-\sigma^2)(1-\sigma^2)+Sk^2(7-\sigma^2)(3-\sigma^2)]}{4\sigma^2[(1-S)\sigma^2-Sk^2(3-\sigma^2)]} + \frac{[8(1-S)-5Sk^2]\omega k^2}{4(1-S+Sk^2)}, \tag{2.15}$$

$$\alpha_4 = \frac{\omega k^2}{2}\left[\frac{(1-S-Sk^2)(1-\sigma^2)^2}{(1-S-4Sk^2)\sigma^2} + \frac{4(1-S)+7Sk^2}{1-S+Sk^2}\right], \tag{2.16}$$

$$\alpha_5 = \omega k\sigma, \tag{2.17}$$

where $\omega = \omega(k)$ is the dispersion relation (2.8), and are recovered in the present formulation. In particular, the cubic coefficients coincide with those obtained in *strictly* inviscid formulations (Pierce and Knobloch [1994]; see also Miles [1993], Hansen and Alstrom [1997] and references therein). The coefficient α_3 diverges at (excluded) resonant wavenumbers satisfying $\omega(2k) = 2\omega(k)$. The last two terms describe the coupling to the mean flow in the bulk (be it viscous or inviscid in origin) in terms of (a local average $\langle\cdot\rangle^x$ of) the streamfunction ψ^m for this flow and the associated free surface elevation f^m. The coefficients of these terms and the function g are given

by

$$\alpha_6 = \frac{k\sigma}{2\omega}, \quad \alpha_7 = \frac{\omega k(1-\sigma^2)}{2\sigma}, \quad g(y) = \frac{2\omega k \cosh[2k(y+1)]}{\sinh^2 k}.$$

The new terms are therefore conservative, implying that at leading order the mean flow does not extract energy from the system. This result is consistent with the small steepness of the associated surface displacement and its small speed compared with the speed $|\nabla\psi|$ due to the surface waves. The mean flow variables in the bulk depend weakly on time but strongly on both x and y, and evolve according to the equations

$$\begin{aligned} &\psi^m_{xx} + \psi^m_{yy} = \Omega^m\,, \\ &\Omega^m_t - [\psi^m_y + (|A|^2 - |B|^2)g(y)]\Omega^m_x + \psi^m_x \Omega^m_y = C_g(\Omega^m_{xx} + \Omega^m_{yy})\,, \end{aligned} \tag{2.18}$$

$$\psi^m_x - f^m_t = \beta_1(|B|^2 - |A|^2)_x\,, \quad \psi^m_{yy} = \beta_2(|A|^2 - |B|^2)\,, \quad \text{at } y = 0\,, \tag{2.19}$$

$$\begin{aligned} (1-S)f^m_x - Sf^m_{xxx} - \psi^m_{yt} + C_g(\psi^m_{yyy} - 3\psi^m_{xxy}) \\ = -\beta_3(|A|^2 + |B^2)_x\,, \quad \text{at } y = 0\,, \end{aligned} \tag{2.20}$$

$$\begin{aligned} &\int_0^L \Omega^m_y\, dx = \psi^m = 0\,, \quad \text{at } y = -1\,, \\ &\psi^m_y = -\beta_4 [iA\bar{B}e^{2ikx} + \text{c.c.} + |B|^2 - |A|^2]\,, \quad \text{at } y = -1\,, \end{aligned} \tag{2.21}$$

$$\psi^m(x+L,y,t) = \psi^m(x,y,t)\,, \quad f^m(x+L,t) = f^m(x,t)\,, \tag{2.22}$$

subject to the constraint

$$\int_0^L f^m(x,t)\, dx = 0\,. \tag{2.23}$$

Here

$$\begin{aligned} &\beta_1 = 2\omega/\sigma\,, && \beta_2 = 8\omega k^2/\sigma\,, \\ &\beta_3 = (1-\sigma^2)\omega^2/\sigma^2\,, && \beta_4 = 3(1-\sigma^2)\omega k/\sigma^2. \end{aligned}$$

Thus the mean flow is forced by the surface waves in two ways. The right sides of the boundary conditions (2.19a) and (2.20) provide a *normal forcing mechanism*; this mechanism is the only one present in strictly inviscid theory (Davey and Stewartson [1974]; Pierce and Knobloch [1994]) and does not appear unless the aspect ratio is large. The right sides of the boundary conditions (2.19b) and (2.21c) describe two *shear forcing mechanisms*, a

tangential stress at the free surface and a tangential velocity at the bottom wall. Note that, as in the simpler example considered in §1, neither of these forcing terms vanishes in the limit of small viscosity (i.e., as $C_g \to 0$). The shear nature of these forcing terms leads us to retain the viscous term in (2.18b) even when C_g is quite small. In fact, when C_g is very small, the effective Reynolds number of the mean flow is quite large. Thus the mean flow itself generates additional boundary layers near the top and bottom of the container, and these must be thicker than the original boundary layers for the validity of the analysis. This puts an additional restriction on the validity of the equations (Vega, Knobloch, and Martel [2001]). There is a third, less effective but inviscid, volumetric forcing mechanism associated with the second term in the vorticity equation (2.18b), which looks like a horizontal force $(|A|^2 - |B|^2)g(y)\Omega^m$ and is sometimes called the *vortex force*. This term plays an important role in the generation of Langmuir circulation (Leibovich [1983]). Although this term vanishes in the absence of mean flow, it can change the stability properties of the flow and enhance or limit the effect of the remaining forcing terms. However, this is not the case in the limit considered in §3 below.

In the following we refer to Eqs. (2.11)–(2.13) and (2.18)–(2.23) as the general coupled amplitude-mean-flow (GCAMF) equations. These equations differ from the exact equations forming the starting point for the analysis in the presence of the forcing terms in the boundary conditions (2.19)–(2.21), and in two essential simplifications: the fast oscillations associated with the surface waves have been filtered out, and the boundary conditions are applied at the unperturbed location of the free surface, $y = 0$. The forcing terms capture completely the effect of the primary viscous boundary layers on the bulk.

The GCAMF equations are invariant under reflection,

$$\psi^m \to -\psi^m\,, \quad \Omega^m \to -\Omega^m\,, \quad A \leftrightarrow B\,, \quad x \to -x\,, \tag{2.24}$$

and hence admit reflection-symmetric solutions. The simplest such solutions are the spatially uniform standing waves given by $A = B = Re^{i\theta}$, where θ is a constant and the amplitude R is given by

$$\delta^2 + \left[d + (\alpha_3 - \alpha_4)R^2\right]^2 = \alpha_5^2\mu^2\,,$$

with an associated reflection-symmetric streaming flow that is periodic in x with period π/k (see Eq. (2.21c)). Since this mean flow does not couple to the amplitudes A, B (i.e., the mean flow terms are absent from Eqs. (2.11)–(2.12)), the presence of this flow does not affect the standing waves. These much-studied waves bifurcate from the flat state at

$$\mu = \mu_c \equiv \frac{(\delta^2 + d^2)^{1/2}}{|\alpha_5|}\,,$$

and do so supercritically if $d < 0$ and subcritically if $d > 0$, see Fig. 2.3. Note that μ can be of order μ_c without violating the conditions for the validity of

the GCAMF equations, and that these equations describe correctly both cases $d < 0$ and $d > 0$. In the former case, the waves are stable near threshold, but may lose stability at finite amplitude through the action of the mean flow as the forcing amplitude increases. Like the secondary saddle-node bifurcation which stabilizes the spatially uniform standing waves when $d > 0$ (see Fig. 2.3), this bifurcation is well within the regime of validity of the GCAMF equations. Thus the mean flow is involved only in possible *secondary* instabilities of the primary standing wave branch.

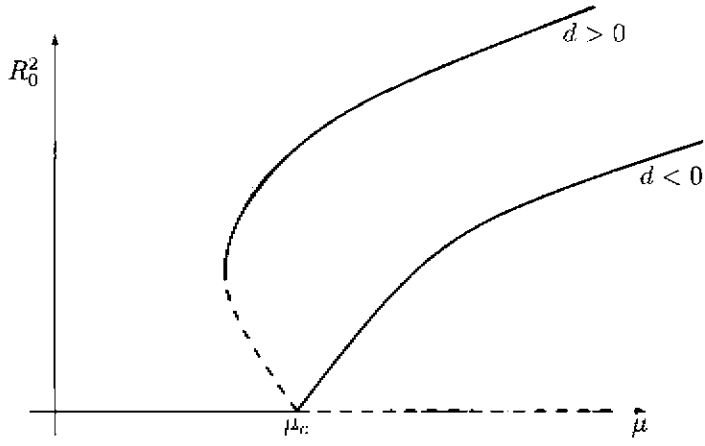

FIGURE 2.3. The primary bifurcation from the flat state to spatially uniform standing wave solutions. The GCAMF equations describe correctly all states with $|\mu - \mu_c| \sim \mu_c$, including the secondary saddle-node bifurcation present when $d > 0$ and the stable solutions beyond it.

The special case $d = 0$ (zero detuning) and $\mu = \mu_c$ defines a codimension-two point for the analysis since both L (or equivalently ω) and μ must be chosen appropriately. In this case the direction of branching is determined by higher order terms neglected in the analysis, such as the real parts of the coefficients of the cubic terms, and this is so for sufficiently small but nonzero values of d as well. In other words, the limit $d \to 0$ (although well-defined within the GCAMF equations) may not describe correctly the corresponding behavior of the underlying fluid equations appropriately close to threshold, i.e., for $|\mu - \mu_c| \ll \mu_c$. However, even in this case the GCAMF equations capture correctly any secondary instabilities involving the mean flow, provided these occur at $\mu \sim \mu_c$. A similar remark applies to other codimension-two points as well.

3 Gravity-Capillary Waves in Moderately Large Aspect-Ratio Containers

The GCAMF equations describe small amplitude slowly varying wavetrains whenever the parameters C_g, L^{-1} and μ are small, but otherwise unrelated to one another. Any relation between them will therefore lead to further simplification. To derive such simplified equations we consider the distinguished limit

$$\delta L^2/\alpha = \Delta \sim 1\,, \quad dL^2/\alpha = D \sim 1\,, \quad \mu L^2/\alpha \equiv M \sim 1\,, \tag{3.1}$$

with $1 \lesssim k \lesssim |\ln C_g|$, and $|\ln C_g|$ taken for simplicity to be $O(1)$ as well. The simplified equations will then be formally valid for $1 \ll L \ll C_g^{-1/2}$ if $k \sim 1$. These are derived under the assumption $1 - S \sim 1$ using a multiple scale method with x and t as *fast* variables and

$$\zeta = x/L\,, \qquad \tau = t/L\,, \qquad T = t/L^2 \tag{3.2}$$

as *slow* variables. In terms of these variables the local horizontal average $(\cdot)^x$ becomes an average over the fast variable x. Note that assumption (3.1) imposes an implicit relation between L and C_g. When $1 - S \sim 1$ the nearly inviscid and viscous mean flows can be clearly distinguished from one another as discussed in §2, and the viscous mean flow can be identified by taking appropriate averages of the whole mean flow over an intermediate timescale τ, i.e., the mean flow variables ψ^m, Ω^m and f^m take the form

$$\psi^m(x,y,\zeta,\tau,T) = \psi^v(x,y,\zeta,T) + \psi^i(x,y,\zeta,\tau,T)\,, \tag{3.3}$$

$$\Omega^m(x,y,\zeta,\tau,T) = \Omega^v(x,y,\zeta,T) + \Omega^i(x,y,\zeta,\tau,T)\,, \tag{3.4}$$

$$f^m(x,\zeta,\tau,T) = f^v(x,\zeta,T) + f^i(x,\zeta,\tau,T)\,, \tag{3.5}$$

with

$$\left|\int_0^\tau \psi_x^i\,d\tau\right| + \left|\int_0^\tau \psi_\zeta^i\,d\tau\right| - \left|\int_0^\tau \psi_y^i\,d\tau\right| - \left|\int_0^\tau \Omega^i\,d\tau\right| + \left|\int_0^\tau f^i\,d\tau\right| \tag{3.6}$$

bounded as $\tau \to \infty$. Thus the nearly inviscid mean flow is purely oscillatory (i.e., it has a zero mean) on the timescale τ. Since its frequency is of the order of L^{-1} (see (3.2)), which is large compared with C_g, the inertial term for this flow is large in comparison with the viscous terms (see Eq. (2.18)), except in two *secondary* boundary layers, of thickness of the order of $(C_g L)^{1/2}$ ($\ll 1$), attached to the bottom plate and the free surface. Note that, as required for the consistency of the analysis, these boundary layers are much thicker than the *primary* boundary layers associated with the surface waves (see Fig. 2), which provide the boundary conditions (2.19)–(2.21) for the mean flow. Moreover, the width of these secondary

boundary layers remains small as $\tau \to \infty$ and (to leading order) the vorticity of this nearly inviscid mean flow remains confined to these boundary layers. This is because, according to condition (3.6), the nearly inviscid mean flow is purely oscillatory on the timescale τ. Consequently, condition (3.6) is essential for the validity of the analysis that follows, and the mathematical definition of the nearly inviscid mean flow through Eqs. (3.3)-(3.6) is the only consistent one; without this condition vorticity would diffuse outside the boundary layers and affect the structure of the whole 'nearly inviscid' solution even at leading order. In fact, vorticity does diffuse (and is convected) from the boundary layers, but this vorticity transport is included in the viscous mean flow. The vorticity associated with the nearly inviscid mean flow is readily seen to be $o(\cdot)$, at most, the order of

$$\big||A|^2 - |B|^2\big| \quad \text{and} \quad \big(|A|^2 + |B|^2\big)(C_g L)^{-1/2}$$

in the upper and lower secondary boundary layers, respectively; the jump in the associated streamfunction ψ^i across each boundary layer is $O(C_g L)$ times smaller. This jump only affects higher order terms; as a consequence the secondary boundary layers can be completely ignored and no additional contributions to the boundary conditions on the nearly inviscid flow need be included in (2.19) and (2.21). Outside these boundary layers, the complex amplitudes and the flow variables associated with the nearly inviscid mean flow are expanded as

$$(A, B) = L^{-1}(A_0, B_0) + L^{-2}(A_1, B_1) + \cdots, \tag{3.8}$$

$$(\psi^i, f^i, \Omega^i) = L^{-2}(\phi_0^i, F_0^i, 0) + L^{-3}(\phi_1^i, F_1^i, W_0^i) + \cdots, \tag{3.9}$$

$$(\psi^v, f^v, \Omega^v) = L^{-2}(\phi_0^v, 0, W_0^v) + L^{-3}(\phi_1^v, F_0^v, W_1^v) + \cdots. \tag{3.10}$$

Substitution of (3.1) (3.6), (3.8)-(3.10) into (2.11) (2.23) leads to the following:

(i) From (2.18) (2.21), at leading order,

$$\phi_{0xx}^i + \phi_{0yy}^i = 0 \text{ in } -1 < y < 0, \quad \phi_0^i = 0 \text{ at } y = -1, \quad \phi_{0x}^i = 0 \text{ at } y = 0,$$

together with $F_{0x}^i = 0$. Thus

$$\phi_0^i = (y+1)\Phi_0^i(\zeta, \tau, T), \quad F_0^i = F_0^i(\zeta, \tau, T).$$

At second order, the boundary conditions (2.19a) and (2.20) yield

$$\phi_{1x}^i(x, 0, \zeta, \tau, T) = F_{0\tau}^i - \Phi_{0\zeta}^i + \beta_1(|B_0|^2 - |A_0|^2)_\zeta,$$
$$(1-S)F_{1x}^i - SF_{1xxx}^i = \Phi_{0\tau}^i - (1-S)F_{0\zeta}^i - \beta_3(|A_0|^2 + |B_0|^2)_\zeta$$

at $y = 0$. Since the right hand sides of these two equations are independent of the fast variable x and both ϕ_1^i and F_1^i must be bounded in x, it follows

that

$$\begin{aligned} \Phi^i_{0\zeta} - F^i_{0\tau} &= \beta_1(|B_0|^2 - |A_0|^2)_\zeta\,, \\ \Phi^i_{0\tau} - v_p^2 F^i_{0\zeta} &= \beta_3(|A_0|^2 + |B_0|^2)_\zeta\,, \end{aligned} \tag{3.12}$$

where

$$v_p = (1-S)^{1/2} \tag{3.13}$$

is the phase velocity of long wavelength surface gravity waves. Equations (3.12) must be integrated with the following additional conditions, which result from (2.22)–(2.23) and (3.6),

$$\Phi^i_0(\zeta+1,\tau,T) \equiv \Phi^i_0(\zeta,\tau,T)\,, \quad F^i_0(\zeta+1,\tau,T) \equiv F^i_0(\zeta,\tau,T)\,, \tag{3.14}$$

$$\begin{aligned} &\int_0^1 F^i_0\, d\zeta = 0\,, \\ &\left|\int_0^\tau \Phi^i_{0\zeta}\, d\tau\right| + \left|\int_0^\tau F^i_0\, d\tau\right| = \text{bounded as } \tau\to\infty\,. \end{aligned} \tag{3.15}$$

(*ii*) The leading order contributions to equations (2.11)-(2.12) yield

$$A_{0\tau} - v_g A_{0\zeta} = B_{0\tau} + v_g B_{0\zeta} = 0\,.$$

Thus

$$A_0 = A_0(\xi,T)\,, \quad B_0 = B_0(\eta,T),$$

where ξ and η are the characteristic variables

$$\xi = \zeta + v_g\tau\,, \quad \eta = \zeta - v_g\tau\,. \tag{3.17}$$

Moreover, according to (2.13),

$$A_0(\xi+1,T) \equiv A_0(\xi,T)\,, \quad B_0(\eta+1,T) \equiv B_0(\eta,T)\,. \tag{3.18}$$

Substitution of these expressions into (3.12) followed by integration of the resulting equations yields

$$\begin{aligned} \Phi^i_0 = {} & \frac{\beta_1 v_p^2 + \beta_3 v_g}{v_g^2 - v_p^2}\left[|A_0|^2 - |B_0|^2 - \langle|A_0|^2 - |B_0|^2\rangle^\zeta\right] \\ & + v_p\left[F^+(\zeta+v_p\tau,T) - F^-(\zeta-v_p\tau,T)\right]\,, \end{aligned} \tag{3.19}$$

$$\begin{aligned} F^i_0 = {} & \frac{\beta_1 v_g + \beta_3}{v_g^2 - v_p^2}\left[|A_0|^2 - |B_0|^2 - \langle|A_0|^2 + |B_0|^2\rangle^\zeta\right] \\ & + \left[F^+(\zeta+v_p\tau,T) + F^-(\zeta-v_p\tau,T)\right]\,, \end{aligned} \tag{3.20}$$

where $\langle\cdot\rangle^{\zeta}$ denotes the mean value in the slow spatial variable ζ, i.e.,

$$\langle G\rangle^{\zeta} = \int_0^1 G\, d\zeta\,, \tag{3.21}$$

and the functions $F^{\pm}$ are such that

$$F^{\pm}(\zeta + 1 \pm v_p\tau, T) \equiv F^{\pm}(\zeta \pm v_p\tau, T)\,, \quad \langle F^{\pm}\rangle^{\zeta} = 0\,. \tag{3.22}$$

The particular solution of (3.19)–(3.20) yields the usual inviscid mean flow included in nearly inviscid theories (see Pierce and Knobloch [1994] and references therein); the averaged terms are a consequence of the conditions (3.15), i.e., of volume conservation (cf. Pierce and Knobloch [1994]) and the requirement that the nearly inviscid mean flow has a zero mean on the timescale τ; the latter condition is never imposed in strictly inviscid theories but is essential in the limit we are considering, as explained above. To avoid the breakdown of the solution (3.19)–(3.20) at $v_p = v_g$ we assume that

$$|v_p - v_g| \sim 1\,. \tag{3.23}$$

The functions $F^{\pm}$ remain undetermined at this stage. In fact, they are not needed below because the evolution of both the viscous mean flow and the complex amplitudes is decoupled from these functions. However, at next order one finds that $F^{\pm}$ remain constant on the timescale T, but decay exponentially due to viscous effects (resulting from viscous dissipation in the secondary boundary layer attached to the bottom plate) on the timescale $t \sim (L/C_g)^{1/2}$.

(*iii*) The evolution equations for A_0 and B_0 on the timescale T are readily obtained from equations (2.11)–(2.13), invoking (3.1)–(3.6), (3.19)–(3.20), (3.22) and eliminating secular terms (i.e., requiring $|A_1|$ and $|B_1|$ to be bounded on the timescale τ):

$$\begin{aligned} A_{0T} =& \mathrm{i}\alpha A_{0\xi\xi} - (\Delta - \mathrm{i}D)A_0 \\ &+ \mathrm{i}\left[(\alpha_3 + \alpha_8)|A_0|^2 - \alpha_8\langle|A_0|^2\rangle^{\xi} - \alpha_4\langle|B_0|^2\rangle^{\eta}\right]A_0 \\ &+ \mathrm{i}\alpha_5 M(\bar{B}_0)^{\eta} - \mathrm{i}\alpha_6\int_{-1}^{0} g(y)\langle\langle\phi_{0y}^{v}\rangle^{x}\rangle^{\zeta}\, dy\, A_0\,, \end{aligned} \tag{3.24}$$

$$\begin{aligned} B_{0T} =& \mathrm{i}\alpha B_{0\eta\eta} - (\Delta + \mathrm{i}D)B_0 \\ &+ \mathrm{i}\left[(\alpha_3 + \alpha_8)|B_0|^2 - \alpha_8\langle|B_0|^2\rangle^{\eta} - \alpha_4\langle|A_0|^2\rangle^{\xi}\right]B_0 \\ &+ \mathrm{i}\alpha_5 M(\bar{A}_0)^{\xi} - \mathrm{i}\alpha_6\int_{-1}^{0} g(y)\langle\langle\phi_{0y}^{v}\rangle^{x}\rangle^{\zeta}\, dy\, B_0\,, \end{aligned} \tag{3.25}$$

subject to (3.18). Here ξ and η are the comoving variables defined in (3.17), and $\langle\cdot\rangle^{x}$, $\langle\cdot\rangle^{\zeta}$, $\langle\cdot\rangle^{\xi}$ and $\langle\cdot\rangle^{\eta}$ denote mean values over the variables x, ζ, ξ and η, respectively. Note that ζ averages over functions of A_0 are equivalent

to ξ averages, while those over functions of B_0 are equivalent to η averages. The real coefficient α_8 is given by

$$\alpha_8 = [\alpha_6(2\omega/\sigma)(\beta_1 v_p^2 + \beta_3 v_g) + \alpha_7(\beta_1 v_g + \beta_3)]/(v_g^2 - v_p^2)\,.$$

Eqs. (3.24)–(3.25) are independent of $F^{\pm}$ because of the second condition in (3.22).

Since

$$\langle |A_0|^2 - |B_0|^2 \rangle^{\tau} = \langle |A_0|^2 \rangle^{\xi} - \langle |B_0|^2 \rangle^{\eta} \to 0 \quad \text{as } T \to \infty$$

the long time behavior of the viscous mean flow is described by

$$\phi^v_{0xx} + \phi^v_{0yy} = W^v_0 \quad \text{in } -1 < y < 0\,, \tag{3.27}$$

$$W^v_{0T} - \phi^v_{0y} W^v_{0x} + \phi^v_{0x} W^v_{0y} = Re^{-1}(W^v_{0xx} + W^v_{0yy}) \quad \text{in } -1 < y < 0\,, \tag{3.28}$$

$$\phi^v_{0x} = \phi^v_{0yy} = 0 \quad \text{at } y = 0\,, \tag{3.29}$$

$$\langle\langle W^v_{0y} \rangle^x \rangle^{\zeta} = \phi^v_0 = 0 \quad \text{at } y = -1\,, \tag{3.30}$$

$$\phi^v_{0y} = -\beta_4 \left[\mathrm{i} \langle A_0 \bar{B}_0 \rangle^{\tau} \mathrm{e}^{2\mathrm{i}kx} + \text{c.c.} \right] \quad \text{at } y = -1\,, \tag{3.31}$$

$$\phi^v_0(x + L, \zeta + 1, y, T) \equiv \phi^v_0(x, \zeta, y, T)\,, \tag{3.32}$$

where the *effective Reynolds number* associated with this viscous mean flow is

$$Re = 1/(C_g L^2)\,. \tag{3.33}$$

Remarks. Some remarks about these equations and boundary conditions are now in order.

a. The viscous mean flow is driven by the short gravity-capillary waves through the inhomogeneous term in the boundary condition (3.31). Since $\langle A_0 B_0 \rangle^{\tau}$ depends on both ζ and T (unless either A_0 or B_0 is spatially uniform) the boundary condition implies that ϕ^v_0 (and hence W^v_0) depends on both the fast and slow horizontal spatial variables x and ζ. This dependence cannot be obtained in closed form (except, of course, in the uninteresting limit $Re \to 0$), and one must resort to numerical computations for realistically large values of L.

b. The higher order oscillatory terms absent from the boundary condition (3.31) oscillate on the intermediate timescale τ, and hence generate secondary boundary layers. However, the contributions from these boundary layers are all subdominant and have no effect at the order considered. Moreover, the free-surface deflection accompanying the viscous mean flow is also small, $f^v \sim L^{-3}$ (see Eq. (3.10)), and so plays no role in the evolution of this flow, as expected of a flow involving the excitation of viscous modes (see §2).

c. The dominant forcing of the viscous mean flow comes from the lower boundary. This forcing vanishes exponentially when $k \gg 1$ leaving only a narrow range of wavenumbers within which such a mean flow is forced while $\delta = O(C_g)$, see Fig. 2.1. Thus in most cases in which a viscous mean flow is present one may assume that

$$\delta = O(C_g^{1/2}) .$$

Note, however, that in fully three-dimensional situations (such as that in Douady, Fauve, and Thual [1989]) in which lateral walls are included a viscous mean flow will be present even when $k \gg 1$ because the forcing of the mean flow in the oscillatory boundary layers along the lateral walls remains.

d. According to the scaling (3.1) and the definitions (2.8), (2.9) and (3.33), the effective Reynolds number Re is large, and ranges from logarithmically large values if $k \sim |\ln C_g$ to $O(C_g^{-1/2})$ if $k \sim 1$. However, even in the latter limit we must retain the viscous terms in (3.28) in order to account for the second boundary conditions in (3.29)-(3.31). Of course, if $Re \gg 1$ vorticity diffusion is likely to be confined to thin layers, but the structure and location of all these layers cannot be anticipated in any obvious way, and one must again rely on numerical computations.

e. Note that the change of variables

$$A_0 = \tilde{A}_0 e^{-i\theta} , \quad B_0 = \tilde{B}_0 e^{i\theta} ,$$

where

$$\theta'(T) = -\alpha_6 \int_{-1}^{0} g(y) \langle \langle \phi_{0y}^{\nu} \rangle^x \rangle^\zeta \, dy ,$$

reduces Eqs. (3.24)- (3.25) to the much simpler form

$$\tilde{A}_{0T} = i\alpha \tilde{A}_{0\xi\xi} - (\Delta + iD)\tilde{A}_0 + i\alpha_5 M \langle \bar{\tilde{B}}_0 \rangle^\eta + i\left[(\alpha_3 + \alpha_8)|\tilde{A}_0|^2 - (\alpha_4 + \alpha_8)\langle |\tilde{A}_0|^2 \rangle^\xi \right] \tilde{A}_0 , \tag{3.36}$$

$$\tilde{B}_{0T} = i\alpha \tilde{B}_{0\eta\eta} - (\Delta + iD)\tilde{B}_0 + i\alpha_5 M \langle \bar{\tilde{A}}_0 \rangle^\xi + i\left[(\alpha_3 + \alpha_8)|\tilde{B}_0|^2 - (\alpha_4 + \alpha_8)\langle |\tilde{B}_0|^2 \rangle^\eta \right] \tilde{B}_0 , \tag{3.37}$$

$$\tilde{A}_0(\xi + 1, T) \equiv \tilde{A}_0(\xi, T) , \quad \tilde{B}_0(\eta - 1, T) \equiv \tilde{B}_0(\eta, T) . \tag{3.38}$$

from which the mean flow is absent. This *decoupling* is a special property of the regime defined by Eq. (3.1). The resulting equations provide perhaps the simplest description of the Faraday system at large aspect ratio, and it is for this reason that they have been extensively studied (Martel, Knobloch, and Vega [2000]). We summarize some of their properties in the next section. ♦

4 Dynamics of the Reduced Equations

In this section we describe some basic properties of the nonlocal equations (3.36)-(3.38) in the invariant subspace $\tilde{A}_0(\cdot, tau) = \tilde{B}_0(\cdot, tau) \equiv C(\cdot, tau)$, say, in which the dynamics are described by the partial differential equation (PDE)

$$C_\tau = \mathrm{i}\alpha C_{xx} - (\Delta + \mathrm{i}D)C + \mathrm{i}\left[(\alpha_3 + \alpha_8)|C|^2 - (\alpha_4 + \alpha_8)\langle|C|^2\rangle\right] C + \mathrm{i}\alpha_5 M\langle\bar{C}\rangle\,, \tag{4.1}$$

subject to periodic boundary conditions. Henceforth the variable x stands for either η or ξ, depending on whether C stands for $\tilde{A}_0$ or $\tilde{B}_0$. Eq. (4.1) describes *standing wave* solutions of Eqs. (3.36)–(3.38). It is possible to show that such standing waves (hereafter SW) are the preferred state at onset (Riecke, Crawford, and Knobloch [1988]) although at larger values of the forcing amplitude such waves may become unstable with respect to perturbations transverse to this subspace (Martel, Knobloch, and Vega [2000]); if this is so the dynamics of Eqs. (3.36) (3.37) and (4.1) will differ.

After an appropriate rescaling (and taking the complex conjugate in (4.1) if $\alpha_3 - \alpha_4 < 0$, and changing the sign of α and d if $\alpha_3 + \alpha_8 < 0$) the standing waves obey an equation of the form

$$C_\tau = \mathrm{i}\alpha C_{xx} - (1 + \mathrm{i}d)C + \mathrm{i}\left[|C|^2 + (\Lambda - 1)\langle|C|^2\rangle\right] C + \mu\langle\bar{C}\rangle\,, \tag{4.2}$$

$$C(x+1,\tau) = C(x,\tau)\,. \tag{4.3}$$

Thus the relative size of the nonlinear terms is measured by the single parameter $\Lambda \equiv 1 - (\alpha_4 + \alpha_8)/(\alpha_3 + \alpha_8)$.

The results of solving equations (3.36) (3.38) and (4.2) (4.3) for identical parameter values are summarized in the bifurcation diagrams shown in Fig. 4.1. These are constructed by noting that equations (4.2)–(4.3) imply

$$\frac{d}{d\tau}\|C\|_{L_2}^2 = -2\|C\|_{L_2}^2 + \mu(\langle\bar{C}\rangle^2 + \text{ c.c.})\,,$$

so that successive intersections of a trajectory with the hypersurface

$$|C|_{L_2}^2 = \tfrac{1}{2}\mu(\langle\bar{C}\rangle^2 + \text{c.c.})$$

are always well defined. In fact this surface contains all the steady states, while each periodic trajectory intersects it at least twice in each period, at the turning points in $|C|_{L_2}$. In the bifurcation diagrams we plot successive *maxima* of $\|C\|_{L_2}$ at each value of μ after transients have died away. In the general case ($|\tilde{A}_0| \neq |\tilde{B}_0|$) we likewise plot the outward intersections with the hypersurface

$$\|\tilde{A}_0\|_{L_2}^2 + \|\tilde{B}_0\|_{L_2}^2 = \mu(\langle\bar{\tilde{A}}_0\rangle\langle\bar{\tilde{B}}_0\rangle + \text{ c.c.})\,,$$

corresponding to maxima in $\|\tilde{A}_0\|_{L_2}^2 + \|\tilde{B}_0\|_{L_2}^2$. Although this procedure for generating bifurcation diagrams is convenient for most purposes it suffers from the disadvantage that it is insensitive to phase drift. Thus additional diagnostics are necessary to identify such drifts, as discussed in detail in Martel, Knobloch, and Vega [2000].

In both cases the first instability produces uniform steady solutions and these subsequently lose stability in a symmetry-breaking pitchfork bifurcation, giving rise to time-independent but spatially nonuniform states. Both these bifurcations preserve the identity $\tilde{A}_0 = \tilde{B}_0$ and hence are common to both sets of equations. Both also preserve the spatial reflection symmetry $\mathcal{R} : x \to -x$. In the case shown in Figs. 4.1a,b the resulting nonuniform but reflection-symmetric states subsequently undergo a Hopf bifurcation and produce a branch of oscillatory solutions. Shortly thereafter chaos sets in, interspersed with nonuniform temporally periodic motion. Some of the observed transitions are the result of crises while others appear to be due to period-doubling cascades. Observe that the details of this behavior differ in the two figures, indicating that the invariant subspace $\tilde{A}_0 = \tilde{B}_0$ does not remain attracting for all values of μ. In the following we restrict attention to the origin of this more complicated dynamical behavior in Eqs. (4.2)–(4.3).

Analysis of the system (4.2)–(4.3) is complicated by the absence of wavenumber-dependent dissipation: the damping is *identical* for all modes. As a result the theorem of Duan, Ly, and Titi [1996] establishing the existence of a finite-dimensional inertial manifold for a nonlocal Ginzburg–Landau of the same type and with the same boundary conditions does not apply. Nonetheless, for the weakly damped nonlinear Schrödinger (NLS) equation with direct external forcing, Ghidaglia [1988] was able to demonstrate the existence of a weak finite-dimensional attractor. This result was improved upon by Wang [1995] who used an energy equation to obtain strong convergence, showing that the attractor is in fact a strong, finite-dimensional, global attractor. Subsequent work (see, e.g., Goubet [1996]; Oliver and Titi [1998]) has dealt with the task of proving additional regularity properties of the attractor. In particular, Oliver and Titi [1998] showed that the global attractor for the weakly damped driven (but local) NLS equation with direct forcing is analytic, indicating that the Fourier expansion of a solution on the attractor converges exponentially fast (as the number of terms is increased) to the exact solution. We believe that these properties continue to hold for the nonlocal equation with parametric forcing, and explain why a simple two-mode truncation of the PDE discussed next describes the PDE dynamics so well over a large range of parameter values.

4.1 Two-Mode Model and Basic Solutions

In view of the fact that both the primary and secondary bifurcations preserve the reflection symmetry $\mathcal{R} : x \to -x$ we focus on the class of

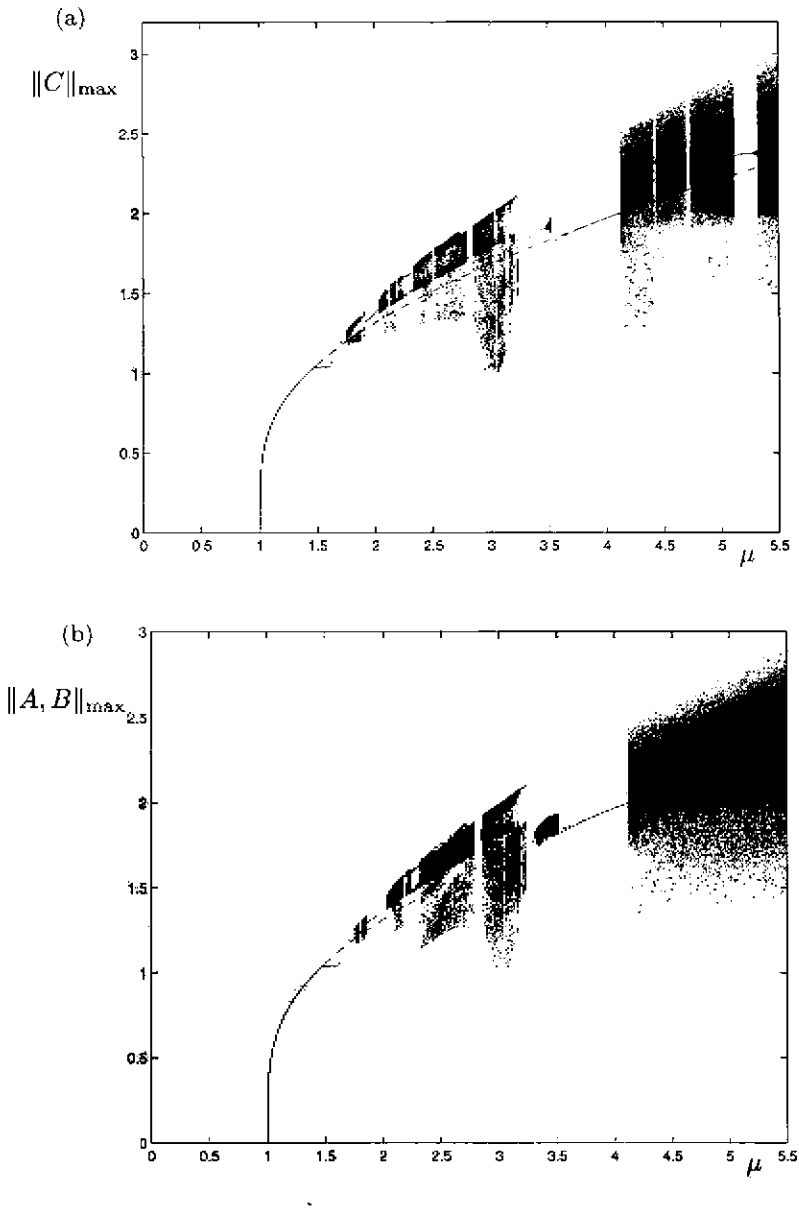

FIGURE 4.1. Bifurcation diagrams for the two systems described in (3.36)-(3.38) and (4.2)–(4.3), with $\alpha = 0.1$, $d = 0$ and $\Delta = 2/3$. Courtesy C. Martel.

reflection-invariant states of the form

$$C(x,\tau) = \frac{1}{\sqrt{2}}c_0(\tau) + \sum_{n=1}^{\infty} c_n(\tau)\cos(2\pi n x)\,. \tag{4.7}$$

Projection of equation (4.2) onto the first two modes then leads to the dynamical system (Higuera, Porter, and Knobloch [2002])

$$\dot{c}_0 = -(1+id)c_0 + i\Lambda(|c_0|^2 + |c_1|^2)\frac{c_0}{2} + i(\bar{c}_0 c_1 - \bar{c}_1 c_0)\frac{c_1}{2} + \mu\bar{c}_0\,, \tag{4.8}$$

$$\dot{c}_1 = -(1+id_1)c_1 + i\Lambda(|c_0|^2 + |c_1|^2)\frac{c_1}{2} + i(\bar{c}_0 c_1 + \bar{c}_1 c_0)\frac{c_0}{2} + i|c_1|^2\frac{c_1}{4}\,, \tag{4.9}$$

where $d_1 = d + 4\pi^2\alpha$. These equations are equivariant under the operations

$$R_0 : (c_0, c_1) \to (-c_0, c_1)\,, \quad R_1 : (c_0, c_1) \to (c_0, -c_1)\,, \tag{4.10}$$

where $R_0 = \hat{\kappa}T_{1/2}$ and $R_1 = T_{1/2}$, and $T_{1/2} : x \to x + \frac{1}{2}$, $C \to C$, and $\hat{\kappa} : C \to -C$ represent two symmetries of the original equations (4.2)–(4.3). These actions generate the group D_2.

Eqs. (4.8)–(4.9) contain three types of fixed points whose properties are summarized below. In what follows we set $d = 0$ (both for simplicity and for comparison with Martel, Knobloch, and Vega [2000]) and write

$$c_0 \equiv x_0 + iy_0\,, \quad c_1 \equiv x_1 + iy_1\,,$$

where x_0, x_1, y_0 and y_1 are all real.

Trivial state (O): This solution has the full symmetry D_2. Its stability is determined by the four eigenvalues $\pm\mu$ 1 and $-1 + i\omega$, where $\omega \equiv 4\pi^2\alpha$. The first two give the growth rate of perturbations within the invariant plane $c_1 = 0$, while the complex conjugate pair describes perturbations within the invariant plane $c_0 = 0$. When $\mu = 1$ there is a supercritical pitchfork bifurcation giving rise to a branch of spatially uniform states U: $c_0 \neq 0$, $c_1 = 0$; note that there are no fixed points of the form $c_0 = 0$, $c_1 \neq 0$.

Uniform steady states (U): These solutions take the form $c_0 \neq 0$, $c_1 = 0$, where

$$|\Lambda|\,|c_0|^2 = 2\sqrt{\mu^2 - 1}\,, \quad \cos 2\vartheta = 1/\mu\,, \tag{4.11}$$

and $c_0 = |c_0|e^{i\vartheta}$, and are invariant under R_1 but not under R_0; when necessary we distinguish between the two R_0-related branches using the notation $U_\pm$ (the $\pm$ reflects the sign of the x_0 coordinate). Since $d = 0$ these solutions are always stable to perturbations within the plane $c_1 = 0$ with the corresponding eigenvalues, s, satisfying

$$(s+1)^2 - (5 - 4\mu^2) = 0\,. \tag{4.12}$$

Note that these eigenvalues are complex when $\mu > \sqrt{5}/2$. Stability with respect to the mode c_1 is described by the characteristic equation

$$(s+1)^2 + \omega^2 + \mu^2 - 1 - \frac{2}{\Lambda}(\mu^2 - 1) - \frac{2\omega}{|\Lambda|}(\Lambda + 1)\sqrt{\mu^2 - 1} = 0\,. \quad (4.13)$$

Thus, when $s = 0$, the uniform states U undergo a pitchfork bifurcation which breaks the R_1 symmetry and produces time-independent nonuniform states with $n = 1$ (NU). Note that because of the form of Eqs. (4.12)–(4.13) Hopf bifurcations are not possible.

Nonuniform steady states (NU): The fixed points NU have no symmetry; consequently, the NU states come in quartets, related by the actions of R_0, R_1, and R_0R_1. Depending on the value of Λ, the NU states may become unstable, with increasing μ, at either a saddle-node or a Hopf bifurcation. If a Hopf bifurcation occurs it generates four symmetry-related periodic orbits. The fate of these and other time-dependent solutions is investigated in the following section.

4.2 Numerical Results

In this section we present the results of a careful numerical investigation of Eqs. (4.8)–(4.9) using a combination of AUTO (Doedel, Champneys, Fairgrieve, Kuznetsov, Sandstede, and Wang [1997]) and XPPAUT (Ermentrout [2000]). In addition to the simple bifurcations mentioned above these equations can exhibit extremely complicated dynamics. We find that over a large range of parameters this complex behavior is organized by a codimension-one heteroclinic connection between the uniform and trivial states, a global bifurcation which can be best understood in the context of a two-parameter study. We therefore set $d = 0$, $\alpha = 0.1$ and vary Λ along with the forcing amplitude μ.

Fig. 4.2 shows the important local bifurcation sets in the (μ, Λ) plane: the $n = 1$ neutral stability curve (labeled SB) and the loci of Hopf and saddle-node (SN) bifurcations on the NU branch which bifurcates from the U state along the neutral curve. Fig. 4.3 shows the bifurcation diagrams obtained on traversing this plane in the direction of increasing μ at several different (but fixed) values of Λ. Fig. 4.2 reveals the presence of two singularities. There is a degeneracy when $\Lambda = 0$: at this value of Λ spatially uniform states exist only at $\mu = 1$ and at no other value of μ. It is thus not surprising that there are many bifurcation sets emanating from the singular point $(\mu, \Lambda) = (1, 0)$. In the present problem there is, in addition, evidence of singular behavior at $\Lambda \simeq -1.1428$, where the amplitude of the NU branch (but not the U branch) becomes infinite. As Λ decreases toward this value the two saddle-node bifurcations on the NU branch (at $\mu \sim 2.33$ and $\mu \sim 5.67$) occur at roughly constant μ values but at larger and larger amplitude (see Fig. 4.3g). When $\Lambda < -1.1428$ these two saddle-node bifurcations no longer occur at all (see Fig. 4.3h).

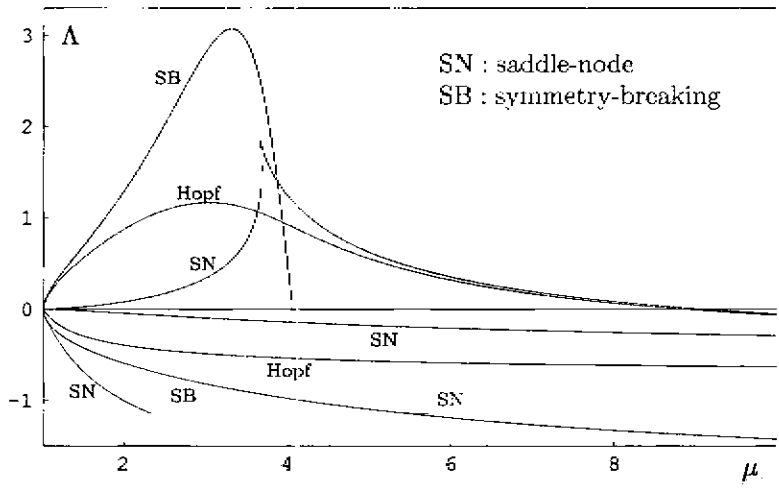

FIGURE 4.2. Local bifurcation sets with $d = 0$ and $\alpha = 0.1$: symmetry-breaking bifurcation (SB) on the U branch, and Hopf and saddle-node (SN) bifurcations on the NU branch. Courtesy M. Higuera and J. Porter.

The bifurcation diagrams of Fig. 4.3 show the U and NU branches, as well as recording the fate of the branches of periodic orbits (when present) generated in Hopf bifurcations on the NU branch (Figs. 4.3a-f). For typical parameter values the NU branch is S-shaped, with the Hopf bifurcations occurring on the lower part. For example, a cut (not shown) at $\Lambda = 1$ barely crosses the locus of Hopf bifurcations but does so twice in quick succession indicating the presence of two Hopf bifurcations back to back (see Fig. 4.2); connecting these bifurcations is a stable branch of periodic orbits. With $\Lambda = 0.9$ (Fig. 4.3a) there is a period-doubling bifurcation on this original branch but the cascade (not shown) is incomplete (there are just two period-doublings followed by two reverse period-doublings). Bifurcation "bubbles" of this type are familiar from problems related to the Shil'nikov bifurcation (Knobloch and Weiss [1981]; Glendinning and Sparrow [1984]). For $\Lambda = 2/3$ (Fig. 4.3b), the value corresponding to Fig. 4.1, there is (presumably) a complete period-doubling cascade and one can easily find a variety of periodic and chaotic attractors (see Fig. 4.4). Evidence that this cascade is not the whole story, however, is provided in Fig. 4.3c. The figure shows that, for $\Lambda = 0.645$, the branch of periodic orbits has split apart, each half terminating in a Shil'nikov-type homoclinic connection with the uniform state. The abruptness of this transition suggests the presence of other periodic orbits with which the original periodic branch is colliding. This interpretation is further supported by a second abrupt transition which occurs by $\Lambda = 0.633$ (Fig. 4.3d); the branch of periodic states produced in the second Hopf bifurcation (at $\mu \simeq 4.8$) now terminates in a

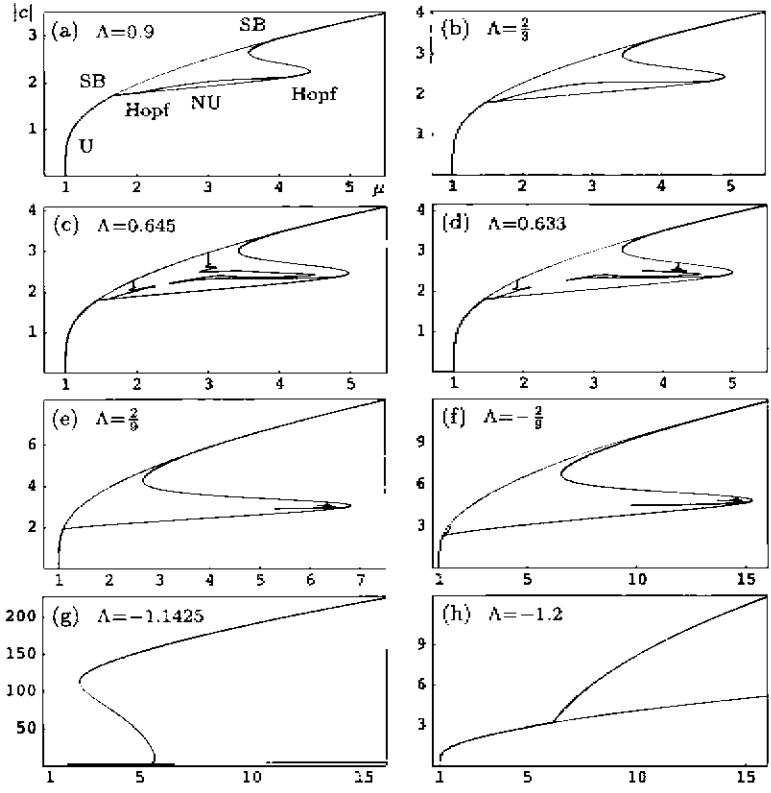

FIGURE 4.3. Series of bifurcation diagrams, $|c| = (|c_0|^2 + |c_1|^2)^{1/2}$ versus μ, for different values of Λ. Stable (unstable) solutions are rendered with thick (thin) lines. Branches of periodic solutions originating in Hopf bifurcations are also shown. Courtesy M. Higuera and J. Porter.

homoclinic bifurcation on the NU states rather than the U states. As Λ is decreased even further (see Fig. 4.3e) the first homoclinic bifurcation (with the U state) moves very close to the initial Hopf bifurcation, occurring at $\mu \simeq 1.112$ when $\Lambda = 2/9$, while the second homoclinic bifurcation (on the NU branch) moves closer to the rightmost saddle-node bifurcation. The branch of periodic solutions corresponding to the former is almost invisible on the scale of the figure. A comparison of Figs. 4.3e and 4.3f shows that when Λ is small in magnitude the bifurcation diagrams on either side of $\Lambda = 0$ are qualitatively similar. The main differences are the change in scale (larger μ values for negative Λ) and the absence of the rightmost symmetry-breaking (SB) bifurcation when $\Lambda < 0$: although the NU branch comes very close to the U branch for large μ the two branches remain

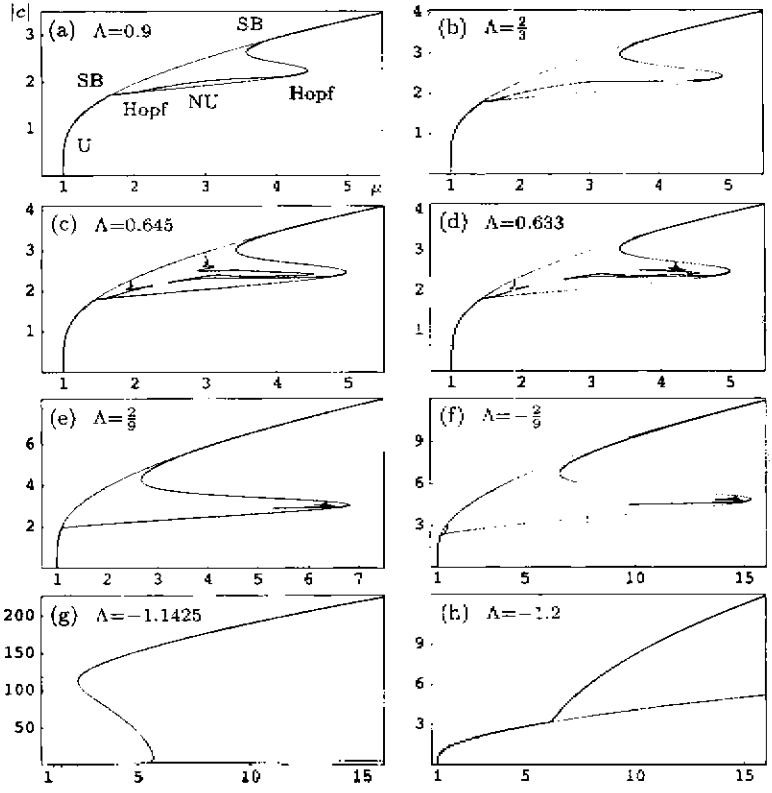

FIGURE 4.3. Series of bifurcation diagrams, $|c| \equiv (|c_0|^2 + |c_1|^2)^{1/2}$ versus μ, for different values of Λ. Stable (unstable) solutions are rendered with thick (thin) lines. Branches of periodic solutions originating in Hopf bifurcations are also shown. Courtesy M. Higuera and J. Porter.

homoclinic bifurcation on the NU states rather than the U states. As Λ is decreased even further (see Fig. 4.3e) the first homoclinic bifurcation (with the U state) moves very close to the initial Hopf bifurcation, occurring at $\mu \simeq 1.112$ when $\Lambda = 2/9$, while the second homoclinic bifurcation (on the NU branch) moves closer to the rightmost saddle-node bifurcation. The branch of periodic solutions corresponding to the former is almost invisible on the scale of the figure. A comparison of Figs. 4.3e and 4.3f shows that when Λ is small in magnitude the bifurcation diagrams on either side of $\Lambda = 0$ are qualitatively similar. The main differences are the change in scale (larger μ values for negative Λ) and the absence of the rightmost symmetry-breaking (SB) bifurcation when $\Lambda < 0$: although the NU branch comes very close to the U branch for large μ the two branches remain

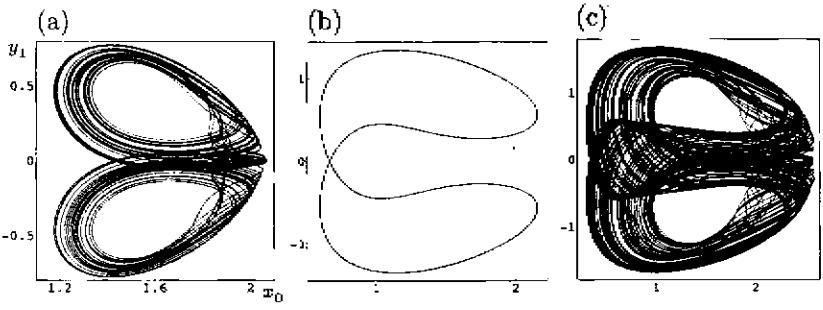

FIGURE 4.4. Attractors for $d = 0$, $\alpha = 0.1$, $\Lambda = 2/3$ and (a) $\mu = 1.86$, (b) $\mu = 2.2$, (c) $\mu = 2.5$. Courtesy M. Higuera and J. Porter.

distinct, in contrast to the situation for $\Lambda > 0$.

It turns out that the interesting periodic and chaotic behavior which one finds for values of Λ such as those used in Figs. 4.3b-f is associated with a *heteroclinic* bifurcation involving both O and U. The bifurcation sets for this global connection, $U \to O \to U$, are shown in Fig. 4.5. In this figure there are three curves of heteroclinic bifurcations which emerge

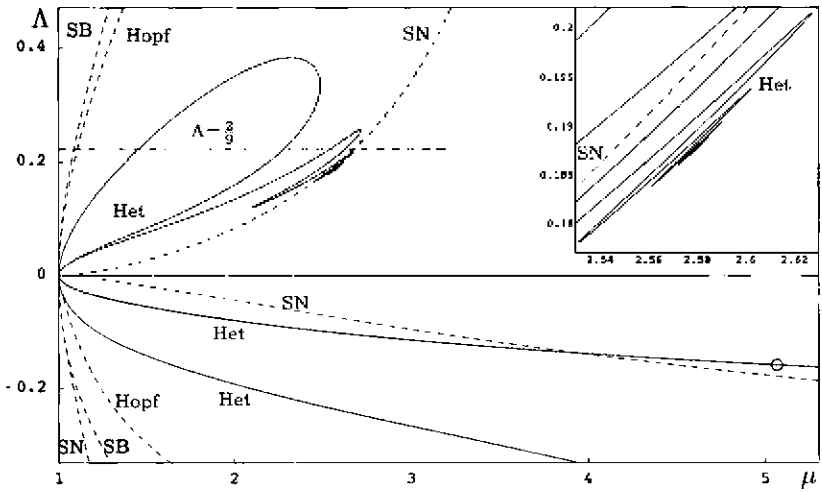

FIGURE 4.5. Heteroclinic (Het) bifurcation sets (solid lines) representing the cycle $U \to O \to U$. The inset shows an enlargement of one of these curves near its termination in the codimension-two heteroclinic cycle $U \to NU \to O \to U$. Note that the cut $\Lambda = 2/9$ passes through four heteroclinic bifurcations. Courtesy M. Higuera and J. Porter.

from $(\mu, \Lambda) = (1, 0)$ into the region $\Lambda > 0$ and three that emerge into

the region $\Lambda < 0$. For $\Lambda > 0$ two of these connect up smoothly forming a loop while the third oscillates back and forth an infinite number of times before terminating in a codimension-two heteroclinic bifurcation point at $(\mu, \Lambda) \simeq (2.5803, 0.1877)$. The heteroclinic cycle at this point involves all three types of fixed points: O, U, and the NU state between the two saddle-node bifurcations on the NU branch. For $\Lambda < 0$ the three curves of heteroclinic bifurcations remain separate (the upper two are almost indistinguishable on the scale of the figure). Two of them continue out to large values of μ (they have been followed to $\mu > 50$) while the third wiggles back and forth before terminating in another codimension-two heteroclinic cycle involving O, U, and NU. This point, $(\mu, \Lambda) \simeq (5.065, -0.159)$, is marked in Fig. 4.5 by a small circle; the wiggles are not visible on this scale. This point differs from the previous codimension-two point for $\Lambda > 0$ in a fundamental way because it involves the small amplitude NU state (after the first Hopf bifurcation) whose stable and unstable manifolds are each two-dimensional. Thus the codimension-two heteroclinic cycle for $\Lambda > 0$ involves three points with one-dimensional unstable manifolds; the connection $O \to U$ is structurally stable (due to the invariance of the uniform plane) while the connections $U \to NU$ and $NU \to O$ are *each* of codimension-one. For $\Lambda < 0$ the connections $O \to U$ and $NU \to O$, are both structurally stable but the third, $U \to NU$, is *itself* of codimension two.

Fig. 4.5 also shows the cut $\Lambda = 2/9$. This cut corresponds to the bifurcation diagram of Fig. 4.3e and crosses the heteroclinic bifurcation set four times. We use this Λ value to investigate further the dynamics associated with this bifurcation. Along this path the first Hopf bifurcation (at $\mu \simeq 1.106$) occurs almost immediately after the birth of the NU branch (see Fig. 4.5). Between this Hopf bifurcation and the leftmost saddle-node bifurcation on the NU branch at $\mu \simeq 2.674$ there are no stable fixed points; in this region one can easily find chaotic attractors, such as those shown in Fig. 4.6, as well as a variety of interesting periodic solutions (see Fig. 4.7).

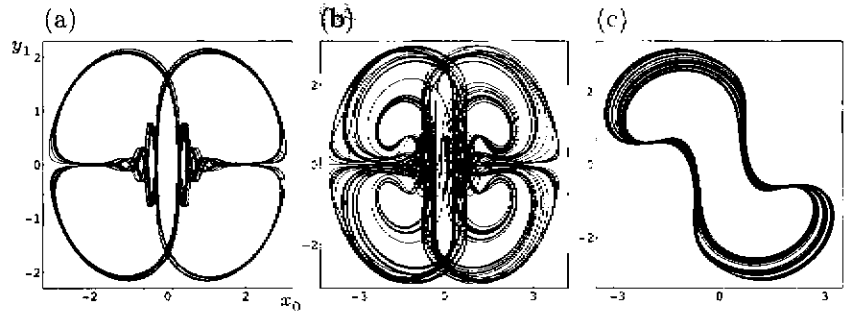

FIGURE 4.6. Chaotic attractors for $d = 0$, $\alpha = 0.1$, $\Lambda = 2/9$ and (a) $\mu = 1.51$, (b) $\mu = 2.0$, (c) $\mu = 2.54$. Courtesy M. Higuera and J. Porter.

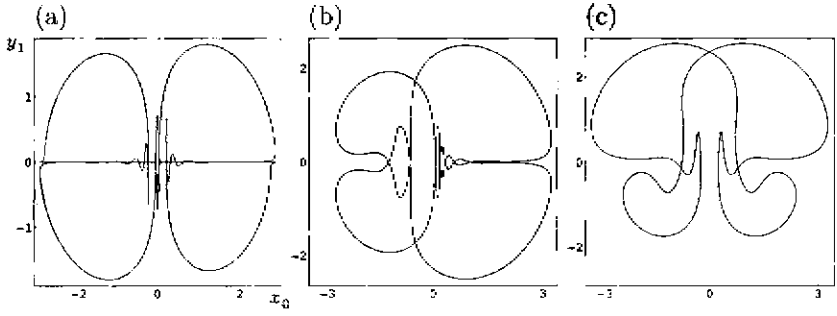

FIGURE 4.7. $\mathbb{Z}_2$-symmetric periodic attractors for $d = 0$, $\alpha = 0.1$, $\Lambda = 2/9$ and (a) $\mu = 1.41$, R_0R_1-symmetry; (b) $\mu = 1.64$, R_1-symmetry; (c) $\mu = 1.875$, R_0-symmetry. Courtesy M. Higuera and J. Porter.

Notice that the periodic orbits in Fig. 4.7 have $\mathbb{Z}_2$ symmetry, i.e., they are invariant under one of the reflections: R_0, R_1, R_0R_1. Although these particular periodic orbits are somewhat exotic (in the sense that they do not belong to one of the basic families of periodic solutions analyzed below but resemble something like the 'multi-pulse' orbits identified in perturbations of the Hamiltonian problem) there are also sequences of simpler periodic orbits which come close to both O and U. These orbits, characterized by their symmetry (or lack thereof) and by the number of oscillations they experience near O, are related in a fundamental way to the heteroclinic connection $U \to O \to U$. A bifurcation diagram obtained by following many of these solutions numerically is displayed in Fig. 4.8, along with four representative orbits. This figure shows the period (half-period for symmetric orbits) as a function of μ.

Two of the branches shown (the ones with lowest period) close on themselves to form isolas but most of the solutions terminate in homoclinic ($U_\perp \to U_\perp$) gluing bifurcations or heteroclinic ($U_\perp \to U_\mp$) symmetry-switching bifurcations. This is evident from the dramatic increase in period which occurs as the periodic orbits approach the fixed points. In the gluing bifurcations two asymmetric periodic orbits come together (using U_+ or U_-) to create a single R_1-symmetric periodic orbit. In the symmetry-switching bifurcations two R_0-symmetric periodic orbits transform (using both U_+ and U_-) into two R_0R_1-symmetric periodic orbits. In this second case the symmetry neither increases nor decreases but switches from one $\mathbb{Z}_2$ symmetry to another.

Under appropriate conditions each of these processes is associated, as in the usual Shil'nikov scenario (Glendinning and Sparrow [1984]; Wiggins [1988]), with cascades of saddle-node and either period-doubling or symmetry-breaking bifurcations; the $\mathbb{Z}_2$-symmetric orbits must undergo symmetry-breaking prior to any period-doubling bifurcations since such orbits do not (generically) have negative Floquet multipliers (Swift and

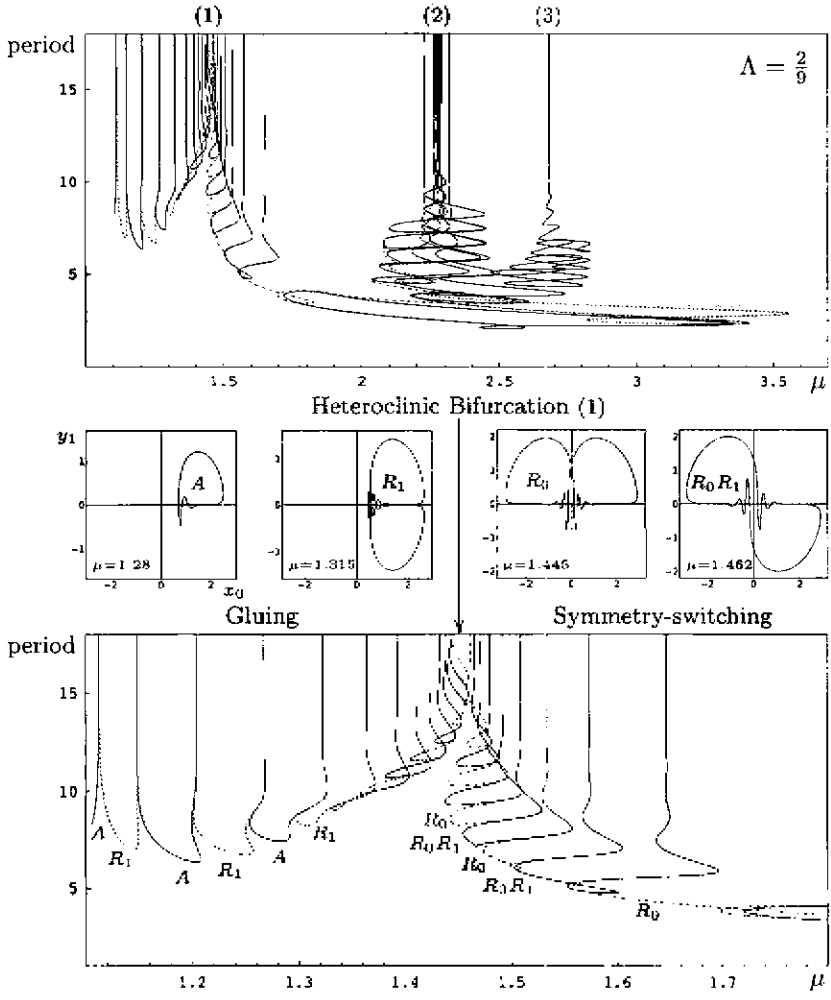

FIGURE 4.8. Cascades of gluing ($A + A \leftrightarrow R_1$) and symmetry-switching ($R_0 + R_0 \leftrightarrow R_0R_1 + R_0R_1$) bifurcations for $d = 0$, $\alpha = 0.1$ and $\Lambda = 2/9$. These accumulate from opposite sides on the principal heteroclinic bifurcations, the first two of which, labeled (1) and (2), are shown (upper panel). At point (3) there is a homoclinic connection to NU. The lower panel shows an enlargement of the region near point (1). The diagrams show the period (half-period) of asymmetric (symmetric) periodic orbits as a function of μ. Courtesy M. Higuera and J. Porter.

Wiesenfeld [1984]). Note also that the way the two branches (e.g., an asymmetric and an R_1-symmetric branch) merge with increasing period

differs from that of the corresponding Shil'nikov problem in three dimensions with symmetry (Glendinning [1984]). This is because the reflection symmetry in the latter case must be a complete inversion (Tresser [1984]; Wiggins [1988]), while in our case the relevant symmetry R_1 is not (see Eq. (4.10)); in particular R_1 does not act on the swirling part of the flow near $U_\pm$ in the plane $c_1 = 0$. In our case the two types of branches oscillate "in phase" around the homoclinic or heteroclinic points as their period increases (cf. Fig. 4.8), while they oscillate "out of phase" in the three-dimensional case with inversion symmetry. These differences between the standard situation and ours are a direct consequence of the fact that our two-mode truncation is four-dimensional, allowing new types of connection that are not possible in three dimensions. Note that in Fig. 4.8 we have only investigated the first two of the main heteroclinic bifurcations (recall that there are four such bifurcations when $\Lambda = 2/9$) and that there are *many* periodic solutions (e.g., those of Fig. 4.7) which have not been shown; these may form isolas or terminate at other, subsidiary, connections. In short, the full situation is extremely complex.

4.3 Comparison with the PDE

Since it is the dynamics of the PDE (4.2)–(4.3) that are of ultimate interest, one would like to understand how faithfully their behavior is represented by a truncated set of ordinary differential equations (ODEs). While there is no a priori reason to assume that a finite number of modes can accurately capture the effect of the nonlinear terms, it turns out that in many problems they do (Knobloch, Proctor, and Weiss [1993]; Doelman [1991]; Rucklidge and Matthews [1996]). Higuera, Porter, and Knobloch [2002] find numerically that these equations frequently have reflection-symmetric attractors (in x) and that these are well described by the restriction to the cosine subspace. In addition, the numerical simulations indicate that the influence of the higher modes is often negligible, particularly for periodic orbits and chaotic attractors which are approximately heteroclinic. Fig. 4.9 shows that the heteroclinic behavior found within the two-mode model (4.8)–(4.9) also occurs in the full PDE.

To examine the influence of higher modes ($n > 1$) on the dynamics we have computed $|c_0|$, $|c_1|$, and $\Sigma_{n=2}^{N}|c_n|$ as functions of time, after first allowing transients to die away. The solutions in Fig. 4.10 represent typical chaotic attractors that can be found for $\Lambda = 2/9$ and $1.5 \lesssim \mu \lesssim 2.8$, together with the time series representing their harmonic content. Notice that in all cases the amplitude of the higher modes (bold curves in the righthand set of panels) remains small, indicating that these modes do not play a significant role in the dynamics.

While such a low-dimensional description is not unexpected for small amplitudes (i.e., near onset at $\mu = 1$) Eqs. (4.2)–(4.3) continue to be described by the two mode truncation even relatively far from the primary bifurcation. Notice that, e.g., for $\Lambda = 2/9$ and $\mu \gtrsim 1.875$ the uniform states are

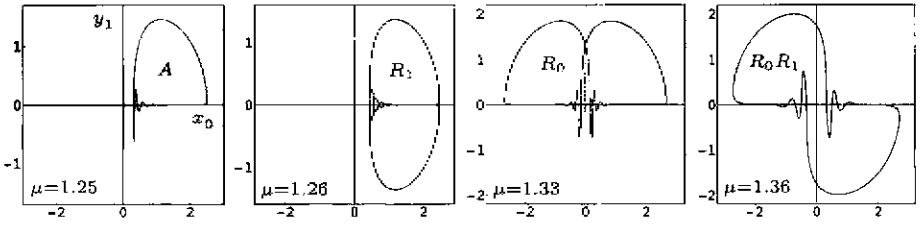

FIGURE 4.9. Stable periodic orbits of the PDE (4.2)–(4.3) with different symmetries for $\Lambda = 2/9$. Gluing and symmetry-switching bifurcations, as in the ODEs, appear to be present. Courtesy M. Higuera and J. Porter.

unstable to at least two nonuniform modes and one might therefore suppose that a two-mode truncation will be of dubious validity. However, we often find that the system (4.8)–(4.9) continues to apply (see Figs. 4.10b,c). This increased range of validity is likely due to the prominence of the heteroclinic bifurcation since for orbits which are approximately heteroclinic the potentially complicated dynamics of the full PDE are controlled mainly by symmetries and by the local properties of the fixed points O and U where most time is spent; recall that O and U are the same in both the PDE (4.2)–(4.3) and the ODE model (4.8)–(4.9). Also important is the fact that due to the spatial averaging of the forcing term in Eq. (4.2) the origin is always stable with respect to nonuniform modes. The higher modes are thus quickly damped under the attracting influence of the trivial state. We conclude that the evident low-dimensional behavior of the PDE (4.2)–(4.3) is related to the presence of the heteroclinic bifurcation involving the origin and its associated cascades. Whenever one is relatively close to these bifurcations in parameter space (see Fig. 4.5) the dynamics will typically be dominated by the many periodic and chaotic attractors associated with them. For parameter values outside of this regime (e.g., $\mu \gtrsim 3$ when $\Lambda = 2/9$) the dynamics are no longer heteroclinic and hence are more likely to involve other modes.

When $\Lambda = 2/3$, the value used in Martel, Knobloch, and Vega [2000] for Fig. 4.1, the heteroclinic bifurcation does not actually occur (see Fig. 4.5), but the dynamics may nonetheless be dominated by the various periodic orbits and related chaotic attractors which exist in nearby regions of parameter space; gluing bifurcations still occur even though the full cascade does not. Fig. 4.11 shows several chaotic attractors for $\Lambda = 2/3$ demonstrating that the dynamics are again dominated by the first two modes. As for $\Lambda = 2/9$, this low-dimensional behavior does not hold for all values of μ and the two-mode ODE model eventually fails. But in contrast to the case $\Lambda = 2/9$, when $\Lambda = 2/3$ this failure can arise for two reasons. The first failure of Eqs. (4.8)–(4.9) is due to a $\mathcal{R}$ symmetry-breaking bifurcation, which occurs at $\mu \sim 3.4$. In this case it is not the two-mode nature of the model

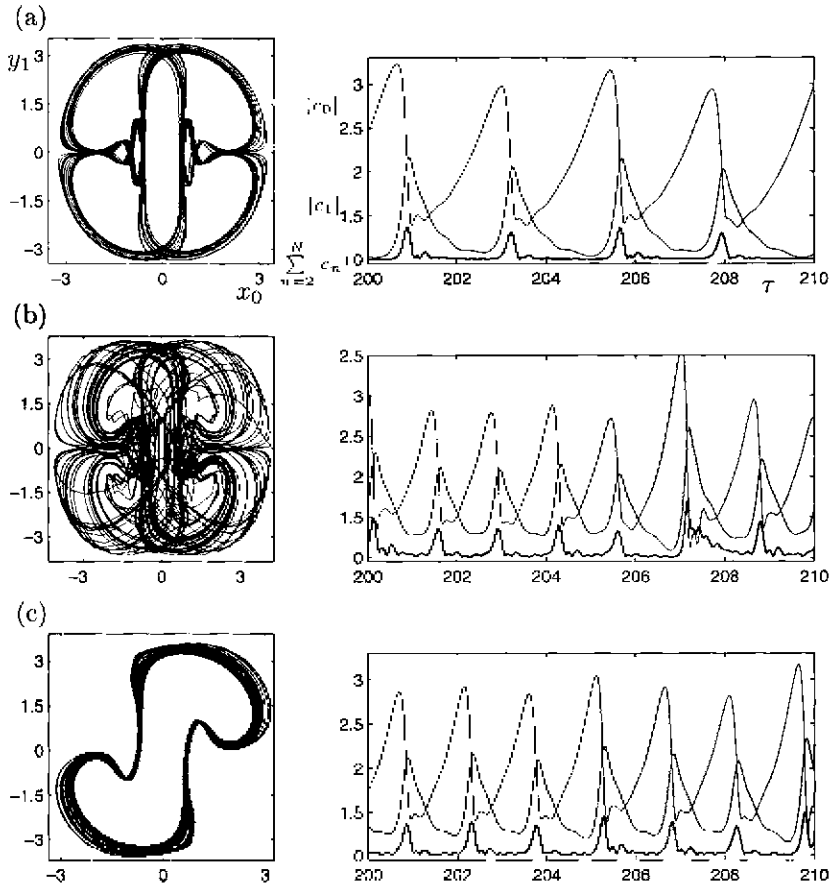

FIGURE 4.10. Relative importance of the Fourier components for $\Lambda = 2/9$: (a) chaotic attractor at $\mu = 1.51$, (b) at $\mu = 2.0$, (c) at $\mu = 2.8$. The lines (———) correspond to $|c_0|$, (———) to $|c_1|$ and (———) to $\Sigma_{n=2}^{N}|c_n|$. Courtesy M. Higuera and J. Porter.

that becomes inappropriate (the uniform state does not lose stability to the $n = 2$ mode until $\mu \simeq 4.093$) but the restriction to the cosine subspace. Fig. 4.12a shows a solution, which possesses low-dimensional character but is not reflection-symmetric and is therefore not contained within the system (4.8)–(4.9). After a narrow interval ($3.4 \lesssim \mu \lesssim 3.46$) the dynamics recover their reflection-symmetric character, and subsequently (see Fig. 4.1) a second window of stable uniform states appears for $3.5 \lesssim \mu \lesssim 4.3$. At $\mu \sim 4.3$ the system becomes abruptly chaotic, with many modes partaking in the dynamics. This situation, however, does not persist uniformly as μ increases further. For example, at $\mu = 4.65$ the trajectories spend a long

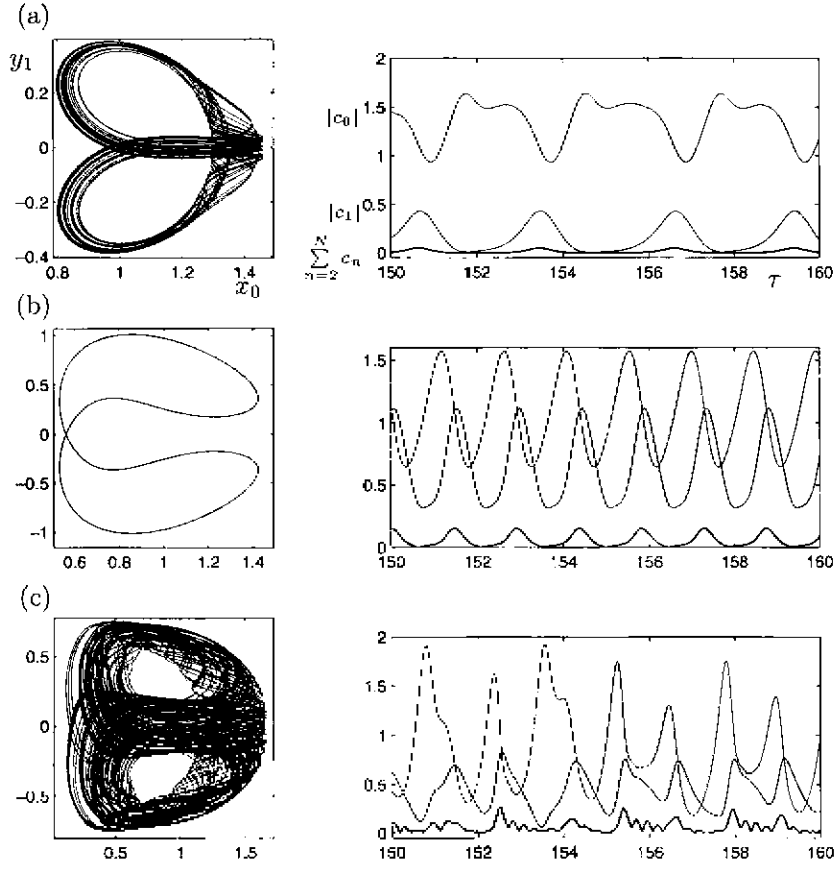

FIGURE 4.11. Relative importance of the different Fourier components when $\Lambda = 2/3$ for chaotic attractors at: (a) $\mu = 1.85$, (b) $\mu = 1.925$, and (c) $\mu = 3.2$. The lines (———) correspond to $|c_0|$, (———) to $|c_1|$ and (———) to $\Sigma_{n=2}^{N}|c_n|$. Courtesy M. Higuera and J. Porter.

time near the invariant *even* subspace ($c_n = 0$ if n is odd), occasionally coming under the influence of unstable periodic orbits in this subspace and being briefly ejected from the even subspace (see Fig. 4.13). These excursions are associated with episodic phase drift of the solution (type I drift in the terminology of Martel, Knobloch, and Vega [2000]). This interesting behavior is reminiscent of the so-called blowout bifurcation (see, e.g., Ashwin, Buescu, and Stewart [1996]). In the present case the attractor is completely contained in the even subspace (with dynamics dominated by the first two even modes, $n = 0, 2$) over a moderately large interval, $5.0 \lesssim \mu \lesssim 6.5$, but loses stability, apparently in the above manner, as μ decreases below $\mu \simeq 5.0$. We remark that blowout bifurcations provide a

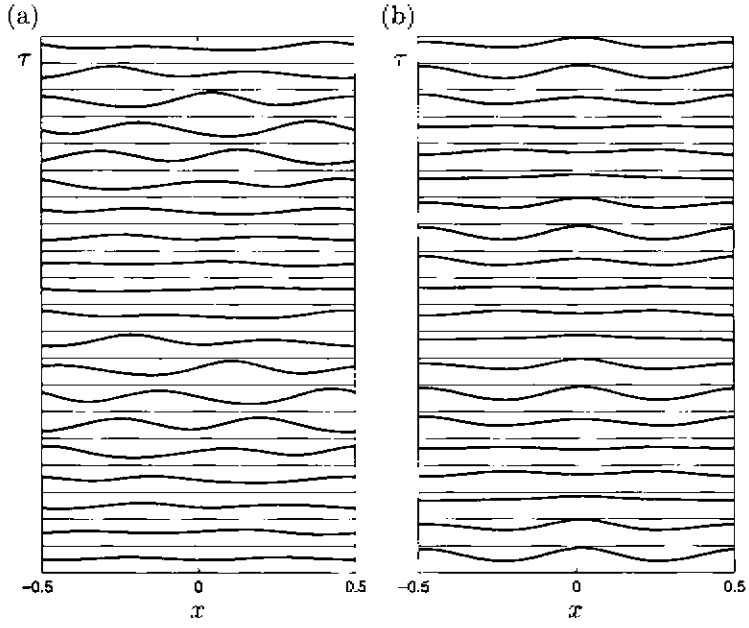

FIGURE 4.12. Space-time diagrams corresponding to (a) a quasiperiodic attractor without reflection symmetry, $A = 2/3$ and $\mu = 3.4$; and (b) a periodic attractor with reflection symmetry, $A = 2/9$ and $\mu = 3.46$. Courtesy M. Higuera and J. Porter.

general mechanism by which attractors in invariant subspaces lose stability with respect to perturbations out of the subspace.

5 Concluding Remarks

In this paper we have summarized the results of a systematic derivation of the amplitude equations describing the evolution of slowly varying wavetrains on the surface of a nearly inviscid liquid excited by small amplitude vertical vibration of its container. Because of the presence of oscillatory viscous boundary layers along the rigid boundaries and the free surface viscous mean flows are driven in the largely inviscid interior of the fluid. These augment any inviscid mean flows that may be present and the two together interact with the parametrically excited waves producing them. This nontrivial interaction between the mean flows and the waves is a consequence of the presence of the hydrodynamic modes which decay, for $C_g \ll 1$, more slowly than gravity-capillary waves, and hence are easily excited by the oscillations. The resulting equations, albeit still complex, provide a significant simplification of the original problem in that the boundary conditions are now applied at the undeformed surface, and the fast oscillation frequency

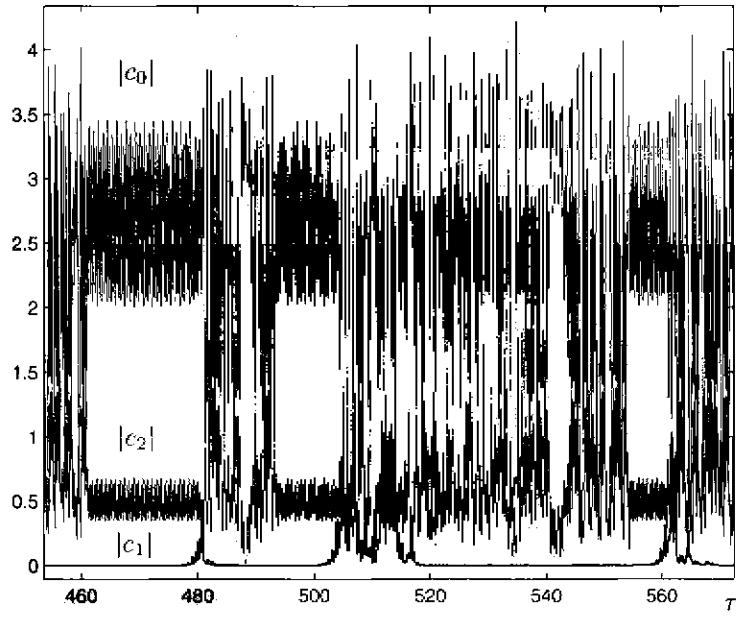

FIGURE 4.13. Norm of the first three modes versus τ for $\Lambda = 2/3$ and $\mu = 4.65$. The thin, medium, and thick lines denote $|c_0|$, $|c_2|$, and $|c_1|$, respectively. Note the episodic excitation of the mode c_1. Courtesy M. Higuera and J. Porter.

associated with the vibration of the container has been eliminated. As part of the analysis explicit expressions for all the coefficients are obtained, as are explicit conditions for the validity of the resulting equations (Vega, Knobloch, and Martel [2001]). As such the resulting equations represent a novel system for the study of pattern formation and subsequent instabilities of the resulting patterns via the excitation of mean flows.

In certain specific cases these equations can be simplified further. We discussed one such case, in which the mean flow decouples from the amplitude equations for the left- and right-traveling waves. The remaining equations are still not trivial, in that they are nonlocal and include both dispersion and damping, although no wavenumber-dependent dissipation. Equations of this type were studied by Martel, Knobloch, and Vega [2000] and provide perhaps the simplest description of the Faraday system in an extended domain under precisely stated conditions. It is important to emphasize that this description *differs* from those obtained by ad hoc procedures. In particular, the usual approach of formulating the problem as an inviscid one at leading order, and adding some damping after the fact to mimic the role of viscosity fails on two levels: it omits the basic mechanisms that drive the (viscous) mean flow (Schlichting [1932]), and it omits the back-reaction of this flow on the waves that are responsible for it. Even the simplest

description of the Faraday system that results includes nonlocal terms in the amplitude equations whose origin can be traced to the fact that amplitude inhomogeities are advected at the group velocity on a timescale that is much faster than the timescale on which the waves equilibrate. An additional nonlocal contribution arises from the requirement that mass be conserved (Pierce and Knobloch [1994]). Since the Reynolds number of the associated flow can be (indeed must be) substantial the equations for this flow must in general be solved numerically as already done in other circumstances (Nicolás, Rivas, and Vega [1997, 1998]).

A careful examination of the analysis that led us to equations (2.11)–(2.23) shows that these in fact apply under the conditions

$$k(|\psi_x| + |\psi_y|) \ll \omega\,, \quad |f| + |f_x| \ll 1\,, \quad L^{-1} \ll k\,, \tag{5.1}$$

or equivalently,

$$k(|A| + |B|) + |f_x^m| \ll 1\,, \quad k|\psi_x^m| \ll \omega\,, \tag{5.2}$$

and the condition

$$L \ll v_g/(\delta + d + \alpha_5\mu)\,. \tag{5.3}$$

Here v_g is the (nondimensional) group velocity of the surface waves, defined in (2.14), α_5 is given in (2.16) and we assumed that the smallest spatial scale is k^{-1}. The condition (5.1) can be stated succinctly as requiring that the nonlinearity be weak and the aspect ratio of the system be large compared to the nondimensional wavelength of the surface waves; the condition (5.3) requires that the terms accounting for inertia and propagation at the group velocity in the amplitude equations (2.11) (2.12) be much larger than the remaining terms. In addition, the requirements

$$(1-S)k^2 + Sk^4 \gg C_g^2\,, \quad k^{\frac{3}{2}}(1-S+Sk^2)^{-\frac{1}{2}} \ll C_g^{-1}\,, \tag{5.4}$$

or equivalently,

$$C_g \ll \omega\,, \qquad C_g^{\frac{1}{2}}\omega^{\frac{3}{2}} \ll 1 - S + (S\omega/C_g)\,. \tag{5.5}$$

are imposed implicitly both on the carrier wavenumber k as well as on all wavenumbers associated with the (viscous) mean flow. These conditions guarantee that the thickness of the associated boundary layers will be small compared to the depth (if $k \ll 1$) or compared to the wavelength (if $k \gg 1$), see Fig. 2.2. Since the lowest wavenumber of the mean flow is $k = 2\pi/L$ the condition (5.4) implies, in particular, that

$$(1-S)L^{-2} + (2\pi)^2 SL^{-4} \gg C_g^2\,. \tag{5.6}$$

Several additional assumptions appear in the course of the analysis (Vega, Knobloch, and Martel [2001]).

It is evident that strictly inviscid treatments of the problem and the powerful techniques that are available for such treatments miss qualitatively important properties of vibrating systems. Similar issues arise in the theory of vibrating liquid bridges (Nicolás and Vega [1996]) and related systems (Higuera, Nicolás, and Vega [2000]), where mean flows generated in the viscous boundary layers can be used to control the amplitude of any convection that may be present. Whether the approach described here for the Faraday system will yield a quantitatively precise description of existing experiments on the Faraday system with nearly inviscid fluids (Ezerskii, Rabinovich, Reutov, and Starobinets [1986]; Douady, Fauve, and Thual [1989]; Tufillaro, Ramshankar, and Gollub [1989]; Kudrolli and Gollub [1997]) remains to be seen, however. Any experiments in a narrow annulus will suffer from effects due to oscillatory boundary layers at the lateral (radial) boundaries which are difficult to minimize. Likewise precise experiments on liquid bridges are difficult under terrestrial conditions, and stability predictions of the type given by Kruse, Mahalov, and Marsden [1999] remain to be confirmed.

The relation between the type of theory described here and earlier work (Kovačič and Wiggins [1992]; Haller and Wiggins [1993, 1995a,b]) on the origin of complex dynamics in the forced weakly damped nonlinear Schrödinger equation is also of interest. This work focused on the near-Hamiltonian limit and exploited generalizations of the Mel'nikov theory to PDEs to establish the presence of a variety of multipulse orbits homoclinic or heteroclinic to a slow manifold. In contrast, our approach has focused on the dynamics substantially farther from this limit. Although much of the dynamical behavior found numerically in the nonlocal parametrically forced damped nonlinear Schrödinger equation derived here could be understood in detail using a two-mode model system, the relation of the cascades of gluing and symmetry-switching bifurcations that appear to be responsible for it to the near-Hamiltonian dynamics analyzed for this class of systems by Kovačič and Wiggins [1992] and Haller and Wiggins [1993, 1995a,b] remains to be examined. Indeed, because of the parametric nature of the forcing (and in particular the resulting symmetry $C \to -C$) the behavior found here bears a greater resemblance to that discussed by Rucklidge and Matthews [1996] in their study of the dynamics of the shearing instability in magnetoconvection than to the damped nonlinear Schrödinger equation with direct forcing. Like our system the former has D_2 symmetry and exhibits global bifurcations involving both the origin (corresponding to the conduction state) and the convective state SS. The latter state is reflection-symmetric and can undergo a pitchfork bifurcation to a tilted convection state STC. From a symmetry point of view these states play the same role as O, U and NU in our problem. The essential difference between our system and that studied by Rucklidge and Matthews lies in the fact that in our case the leading stable eigenvalues of both O and U are complex (the former in the $c_0 = 0$ subspace, and the latter in the $c_1 = 0$ subspace). The dynamical

behavior that results is new and is discussed in detail in Higuera, Porter, and Knobloch [2002] and Porter [2001]. Truncated Galerkin expansions of the type that led us to this behavior have, of course, also been used to study the effect of direct forcing on the sine-Gordon equation, a system closely related to ours. Here, too, the study of the finite-dimensional system proved of substantial help in understanding the PDE simulations (Bishop, Forest, McLaughlin, and Overman [1990]; McLaughlin, Overman, Wiggins, and Xiong [1996]). It should therefore not come as a complete surprise that the two-mode model constructed here captures so much of the behavior found numerically in the PDE (4.2)–(4.3) by Martel, Knobloch, and Vega [2000].

Acknowledgments: We are very grateful for long-term assistance from our colleagues M. Higuera, C. Martel, J. Nicolás and J. Porter with whom the results reported here were obtained. This work was supported in part by the National Aeronautics and Space Administration under Grant NAG3-2152 and by the Spanish Dirección General de Enseñanza Superior under Grant PB97-0556.

References

Abarbanel, H. D. I., D. D. Holm, J. E. Marsden, and T. S. Ratiu [1986], Nonlinear stability analysis of stratified fluid equilibria, *Phil. Trans. Roy. Soc. London A*, 318:349–409.

Ashwin, P., J. Buescu, and I. Stewart [1996], From attractor to saddle: a tale of transverse instability, *Nonlinearity*, 9:703–738.

Batchelor, G. K. [1967], *An Introduction to Fluid Dynamics*, Cambridge Univ. Press.

Bishop, A. R., M. G. Forest, D. W. McLaughlin, and E. A. Overman II [1990], A modal representation of chaotic attractors for the driven, damped pendulum chain, *Phys. Lett. A*, 144:17–25.

Chorin, A. and J. E. Marsden [1979], *A Mathematical Introduction to Fluid Mechanics* Springer-Verlag.

Craik, A. D. D. [1982], The drift velocity of water waves, *J. Fluid Mech.*, 116:187–205.

Davey, A., L. M. Hocking, and K. Stewartson [1974], On nonlinear evolution of three-dimensional disturbances in plane Poiseuille flow, *J. Fluid Mech*, 63:529–536.

Davey, A. and K. Stewartson [1974], On three-dimensional packets of surface waves, *Proc. R. Soc. London, Ser. A*, 338:101–110.

Doedel, E. J., A. R. Champneys, T. F. Fairgrieve, Y. Kuznetsov, B. Sandstede, and X. J. Wang [1997], AUTO 97: Continuation and bifurcation software for ordinary differential equations (available via FTP from directory pub/doedel/auto at ftp.cs.concordia.ca).

Doelman, A. [1991], Finite-dimensional models of the Ginzburg–Landau equation, *Nonlinearity*, 4:231–250.

Douady, S., S. Fauve, and O. Thual [1989], Oscillatory phase modulation of parametrically forced surface waves, *Europhys. Lett.*, 10:309–315.

Duan, J., H. V. Ly, and E. S. Titi [1996], The effects of nonlocal interactions on the dynamics of the Ginzburg–Landau equation, *Z. angew. Math. Phys.*, 47:432–455.

Ermentrout, B. [2000], XPPAUT, Dynamical systems software with continuation and bifurcation capabilities (available via FTP from directory /pub/bardware at ftp.math.pit.edu).

Ezerskii, A. B., M. I. Rabinovich, V. P. Reutov, and I. M. Starobinets [1986], Spatiotemporal chaos in the parametric excitation of a capillary ripple, *Sov. Phys. JETP*, 64:1228–1236.

Fauve, S. [1995], Parametric instabilities, In G. Martínez Mekler and T.H. Seligman, editors, *Dynamics of Nonlinear and Disordered Systems*, pp. 67–115. World Scientific.

Ghidaglia, J. M. [1988], Finite-dimensional behaviour for weakly damped driven Schrödinger equations, *Ann. Inst. H. Poincaré – Anal. Non-Linéaire*, 5:365–405.

Glendinning, P. [1984], Bifurcations near homoclinic orbits with symmetry, *Phys. Lett. A*, 103:163–166.

Glendinning, P. and C. Sparrow [1984], Local and global behavior near homoclinic orbits, *J. Stat. Phys.*, 35:645–696.

Goubet, O. [1996], Regularity of attractor for a weakly damped nonlinear Schrödinger equation, *Appl. Anal.*, 60:99–119.

Haller, G. and S. Wiggins [1993], Orbits homoclinic to resonances: the Hamiltonian case, *Physica D*, 66:298–346.

Haller, G. and S. Wiggins [1995a], N-pulse homoclinic orbits in perturbations of resonant Hamiltonian systems, *Arch. Rat. Mech. Anal.*, 130:25–101.

Haller, G. and S. Wiggins [1995b], Multi-pulse jumping orbits and homoclinic trees in a modal truncation of the damped-forced nonlinear Schrödinger equation, *Physica D*, 85:311–347.

Hansen, P. L. and P. Alstrom [1997], Perturbation theory of parametrically driven capillary waves at low viscosity, *J. Fluid Mech.*, 351:301–344.

Henderson, D. M. and J. W. Miles [1994], Surface-wave damping in a circular cylinder with a fixed contact line, *J. Fluid Mech.*, 275:285–299.

Higuera, M., J. A. Nicolás, and J. M. Vega [2000], Coupled amplitude-streaming flow equations for the evolution of counter-rotating, nearly-inviscid surface waves in finite axisymmetric geometries, *Preprint*.

Higuera, M., J. Porter, and E. Knobloch [2002], Heteroclinic dynamics in the nonlocal parametrically driven Schrödinger equation, *Physica D*, 162:155–187.

Holm, D. D., J. E. Marsden, T. S. Ratiu, and A. Weinstein [1985], Nonlinear stability of fluid and plasma equilibria. *Phys. Rep.*, 123:1–116.

Holm, D. D., J. E. Marsden, and T. S. Ratiu [1986], Nonlinear stability of the Kelvin–Stuart cat's eyes flow, in *Lects. in Appl. Math.*, 23:171–186.

Kakutani, T. and K. Matsuuchi [1975], Effect of viscosity on long gravity waves, *J. Phys. Soc. Japan*, 39:237–246.

Knobloch, E. and R. Pierce [1998], On mean flows associated with travelling water waves, *Fluid Dyn. Res.*, 22:61–71.

Knobloch, E., M. R. E. Proctor, and N. O. Weiss [1993], Finite-dimensional description of doubly diffusive convection, in *Turbulence in Fluid Flows: A Dynamical Systems Approach*, G.R. Sell, C. Foias, and R. Temam (eds), Springer-Verlag, New York, IMA Volumes in Mathematics and its Applications 55, pp. 59–72.

Knobloch, E. and N. O. Weiss [1981], Bifurcations in a model of double-diffusive convection, *Phys. Lett. A*, 85:127–130.

Kovačič, G. and S. Wiggins [1992], Orbits homoclinic to resonances, with an application to chaos in a model of the forced and damped sine-Gordon equation, *Physica D*, 57:185–225.

Kruse, K.-P., A. Mahalov, and J. E. Marsden [1999], On the Hamiltonian structure and three-dimensional instabilities of rotating liquid bridges. *Fluid Dyn. Res.*, 24:37–59.

Kudrolli, A. and J. P. Gollub [1997], Patterns and spatio-temporal chaos in parametrically forced surface waves: A systematic survey at large aspect ratio, *Physica D*, 97:133–154.

Leibovich, S. [1983], On wave-current interaction theories of Langmuir circulations *Ann. Rev. Fluid Mech.*, 15:391–427.

Lewis, D., J. E. Marsden, R. Montgomery, and T. S. Ratiu [1986], The Hamiltonian structure for dynamic free boundary problems, *Physica D*, 18:391–404.

Longuet-Higgins, M. S. [1953], Mass transport in water waves, *Phil. Trans. R. Soc. London, Ser. A*, 245:535–581.

Marsden, J. E. and P. J. Morrison [1984], Noncanonical Hamiltonian field theory and reduced MHD. *Contemp. Math.*, 28:133–150.

Martel, C. and E. Knobloch [1997], Damping of nearly inviscid water waves, *Phys. Rev. E*, 56:5544–5548.

Martel, C., E. Knobloch, and J. M. Vega [2000], Dynamics of counterpropagating waves in parametrically forced systems, *Physica D*, 137:94–123.

McLaughlin, D. W., E. A. Overman II, S. Wiggins, and C. Xiong [1996], Homoclinic orbits in a four-dimensional model of a perturbed NLS equation: A geometric singular perturbation study, in *Dynamics Reported*, vol. 5, Springer-Verlag, New York; p. 190.

Miles, J. W. [1993], On Faraday waves, *J. Fluid Mech.*, 248:671–683.

Miles, J. and D. Henderson [1990], Parametrically forced surface waves, *Ann. Rev. Fluid Mech.*, 22:143–165.

Nicolás, J. A., D. Rivas, and J. M. Vega [1997], The interaction of thermocapillary convection and low-frequency vibration in nearly-inviscid liquid bridges, *Z. Angew. Math. Phys.*, 48:389–423.

Nicolás, J. A., D. Rivas, and J. M. Vega [1998], On the steady streaming flow due to high frequency vibration in nearly-inviscid liquid bridges, *J. Fluid Mech.*, 354:147–174.

Nicolás, J. A. and J. M. Vega [1996], Weakly nonlinear oscillations of axisymmetric liquid bridges, *J. Fluid Mech.*, 328:95–100.

Oliver, M. and E. Titi [1998], Analyticity of the attractor and the number of determining modes for a weakly damped driven nonlinear Schrödinger equation, *Indiana Univ. Math. J.*, 47:49–73.

Phillips, O. M. [1977], *The Dynamics of the Upper Ocean*, Cambridge Univ. Press.

Pierce, R. D. and E. Knobloch [1994], On the modulational stability of traveling and standing water waves, *Phys. Fluids*, 6:1177–1190.

Porter, J. B. [2001], Global bifurcations with symmetry. Ph.D. Thesis, University of California at Berkeley.

Riecke, H., J. D. Crawford, and E. Knobloch [1988], Time-modulated oscillatory convection, *Phys. Rev. Lett.*, 61:1942–1945.

Rucklidge, A. M. and P. C. Matthews [1996], Analysis of the shearing instability in nonlinear convection and magnetoconvection, *Nonlinearity*, 9:311–351.

Schlichting, H. [1932], Berechnung ebener periodischer Grenzschichtströmungen, *Phys. Z.*, 33:327–335.

Swift, J. W. and K. Wiesenfeld [1984], Suppression of period doubling in symmetric systems, *Phys. Rev. Lett.*, 52:705–708.

Tresser, C. [1984], About some theorems by L.P. Shil'nikov, *Ann. Inst. Henri Poincaré – Phys. Theorique*, 40:440–461.

Tufillaro, N. B., R. Ramshankar, and J. P. Gollub [1989], Order-disorder transition in capillary ripples, *Phys. Rev. Lett.*, 62:422–425.

Vega, J. M., E. Knobloch, and C. Martel [2001], Nearly inviscid Faraday waves in annular containers of moderately large aspect ratio, *Physica D*, 154:313–336.

Wang, X. [1995], An energy equation for the weakly damped driven nonlinear Schrödinger equations and its application to their attractors, *Physica D*, 88:167–175.

Wiggins, S. [1988], *Global Bifurcations and Chaos: Analytical Methods*, Springer-Verlag, New York.